Interactions of Contaminating Agents with Building Materials: Literature Review and Preliminary Experiments

Prepared by:

Marcy Brownell, Dr. Mandar Dewoolkar, Dr. Nancy Hayden and Dr. Donna Rizzo
Civil and Environmental Engineering, School of Engineering

Douglas Porter
History Department

University of Vermont, Burlington, VT 05405

Prepared for:

Los Alamos National Laboratory
Materials Science Division
Los Alamos, NM

October 2006

PURPOSE AND OBJECTIVES

The purpose of this project was to evaluate and develop experimental techniques to assist in characterizing the transport of "contaminating agents" into typical historic and modern building materials. This research was conducted to support the overall project objective of developing and verifying analytical models for prediction of long-term fate and transport of chemical or biological agents in building materials, to ultimately assist in the development of effective decontamination strategies. The specific objectives were to:

1. conduct a literature search on building material properties (e.g., density, porosity, permeability) and characterization technologies as related to this project;
2. compile the results of the literature search into a usable format;
3. evaluate state-of-the-art technologies such as X-ray tomography and fluorescent confocal microscopy with respect to their usefulness in characterizing building material properties and interactions with contaminant surrogates;
4. design and conduct experiments to enhance our understanding of transport within building materials (e.g., wicking experiment, contact angle tests); and
5. prepare a report describing methods and summarizing the results.

Scope of Research

The research was conducted at the University of Vermont from May to September 2006. In addition to the literature search, six experimental techniques were evaluated. These techniques included; contact angle tests, wicking tests, dye migration tests, x-ray tomography, fluorescent confocal microscopy, and air permeability mapping. Fluorescent salts, water-soluble dyes and iodine were used as solutes. Water was used as the solvent. Six types of historic and modern building materials were considered; mortar, Indiana limestone, brick, arkose sandstone, Ohio sandstone, and concrete. The dye migration test was conducted on sand/clay mixed media. Physical properties, absorption and hydraulic conductivities of some of these materials were determined in 2005, and these results are included in Appendix A (previously summarized by Ashworth, et al. (2005)).

In this report, relevant results of the literature search are summarized first. Details of materials tested, experimental techniques, results and analysis are presented in the subsequent sections.

SUMMARY OF THE LITERATURE SEARCH

A literature search was conducted to determine properties that are considered important in modeling fluid transport for similar types of building materials used in the experimental investigations. These properties included density, porosity, surface area and hydraulic conductivity and are summarized in Tables 1 through 5. Not all of the properties were measured or reported for each material; therefore there are gaps in the tables. There were also differences in terminology related to porosity. Some literature presented values for porosity, while others referred to it as open porosity. It is likely that both terms refer to the measurable accessible porosity of the sample. Since many of these samples may have some pore space that is inaccessible (i.e., completely closed) to other pores, the authors may have wanted to clearly distinguish between these and accessible pores. In only a few cases, did the researchers report

both an open porosity and porosity (in this case total porosity) terms. In those cases, the open porosity is less than the total porosity, indicating that there some pores exist that are not accessible.

One important point to note is the variability in properties even within the same types of materials. This heterogeneity of materials should not be underestimated and will play an important and often confounding role in contaminant transport and subsequent remediation efforts. It is the most difficult problem in groundwater contaminant transport and remediation issues and will undoubtedly be problematic in building materials as well.

Table 1: Physical properties of concrete from published literature

	Density (kg/m^3)	**Bulk Density (kg/m^3)**	**Open Porosity (%)**	**Porosity (%)**	**Surface Area (m^2/kg)**
Aerated Concrete[3]		752		29.9	1279
Solid Concrete[3]		1867		10.4	527
Concrete[12]	2250		15.80		
Autoclaved Aerated Concrete[20]		385		84	
White Concrete Brick[23]		2420 ± 13	10.9 ± 0.5		
Concrete Brick[23]		2427 ± 25	10.5 ± 0.8		
Cellular Concrete[24]		500 - 600		72	
RANGE	**2250**	**385 - 2427**	**10.5 - 15.8**	**10.4 - 84**	**527 - 1279**

Table 2: Physical properties of brick from published literature

	Density (kg/m^3)	Bulk Density (kg/m^3)	Open Porosity (%)	Porosity (%)	Surface Area (m^2/kg)	Gas Permeability (cm^2)
Fired-Clay (ceramic red) Brick[1]			30			
White Siliceous (lime–sand) Brick[1]			20			
New Red Brick[2]	2000			22.5 - 23.8	400	
Old Light Brick[2]	1800			29.2 - 32.4	10900	
Old Dark Brick[2]	2300			12.0 - 17.7	180	
Brick[3]		1987.4		17.1	507	
Lime Silica Brick[8]	2600	1830	30			3.9×10^{-10}
Clinker Brick[8]	2610	2080	20			6×10^{-11}
Soft Mud Brick[9]				35.7		
Ceramic Brick[12]	2004.8		24.00			
Calcium Silicate Brick[20]		1689		35.9		
Dry-pressed Clay Brick[20]				16.1 - 25.5		
Extruded Clay Brick[20]				7.0 - 27.9		
Red Matt Clay Brick[23]		2024 ± 11	23.2 ± 0.8			
Buff Matt Clay Brick[23]		1788 ± 7	36.4 ± 0.3			
Textured Coated Clay Brick[23]		1869 ± 15	31.6 ± 1.0			
Calcium Silicate Brick[23]		2062 ± 8	24.0 ± 0.3			
Lime Silica Brick[24]		1700 - 1800		35		
Solid Clay Brick[24]		1600				
Red Brick[26]	1730			38		
Brick[28]	1900			29		
RANGE	**1730 - 2610**	**1600 - 2080**	**20 - 36.4**	**7.0 - 38**	**180 - 10900**	**$0.6 - 3.9 \times 10^{-10}$**

Table 3: Physical properties of mortar from published literature

	Density (kg/m^3)	Bulk Density (kg/m^3)	Open Porosity (%)	Porosity (%)	Surface Area (m^2/kg)
Mortar[3]		2738.3		22.6	1.4385×10^4
Cement-sand Mortar[20]		2070		16.7	
Harden Cement Paste[20]		1764		28	
Portland Cement[23]		1857 ± 19	30.0 ± 0.6		
Lime Mortar[23]		1872 ± 9	31.0 ± 0.1		
Masonry Cement[23]		1581 ± 12	42.1 ± 0.4		
Mortar[23]		1675 ± 35	38.7 ± 1.3		
Cement-Lime Mortar[24]		1900			
Lime Mortar[24]		1400			
Kaolin Mortar[26]	~300			~90	
Mortar[28]	1710			31	
Cement Mortar[28]	2050			18	
RANGE	**300 - 2050**	**1400 - 2738**	**30 - 42.1**	**16.7 - 90**	**1.4385×10^4**

Table 4: Physical properties of limestone from published literature

LIMESTONES	Density (kg/m^3)	Bulk Density (kg/m^3)	Open Porosity (%)	Porosity (%)	Surface Area (m^2/kg)	Gas Permeability (cm^2)	Permeability (cm^2)
Biocalcirudite #1[7]		2140	11.71 - 12.45		1060		
Biocalcirudite #2[7]		1920	9.23 - 14.29		550		
Biocalcirudite #3[7]		2030	12.69 - 14.01		980		
Biocalcirudite #4[7]		2320	4.51 - 15.03		1220		
Biocalcirudite #5[7]		1940	17.32 - 27.55		9570		
Biocalcirudite #6[7]		1950	6.46 - 15.75		670		
Biocalcirudite #7[7]		2110	11.81 - 14.14		580		
Biocalcirudite #8[7]		2080	17.49 - 18.58		520		
Biocalcarenite #1[7]		2000	15.03 - 22.57		9640		
Biocalcarenite #2[7]		2250	11.59 - 22.36		9880		
Biocalcarenite #3[7]		2150	13.60 - 18.33		6340		
Biocalcarenite #4[7]		2120	15.69 - 19.73		7800		
Biocalcarenite #5[7]		2220	15.08 - 28.74		7820		
Biocalcarenite #6[7]		2120	12.51 - 17.78		1370		
Biocalcarenite #7[7]		2060	16.32 - 18.50		3350		
Biocalcarenite #8[7]		2250	13.74 - 19.31		6760		
Biomicrite[7]		2000	20.56 - 25.14		12110		
Noto (Italy)[9]				29.04			
Maastricht[13]				50.5 ± 3.1			
Bihacite[14]	2700	1820		32.59			
Pinczow[16]	1640		30.3		2900		
Karsy[16]	1460		42.0		1.54×10^4		
Laspra[17]			28	30	4600		
Hontoria[17]			14.2	19.8	800		
Miocenic[18]				27.73			
Estaillades[20]				32.4 - 32.7			
Ketton[20]				25.1 - 25.2			
Richemont[20]				30.3 - 31.3			
Lépine[20]		2010		24.5			
Salem[20]		2240		17.6			
Anstrude[26]				19.9			4.34×10^{-12}
Tonnerre[26]				13.7			1.68×10^{-10}
Chauvigny[26]				17.4			2.37×10^{-10}
Lavoux[26]				21.8			4.44×10^{-11}
Krensheimer[30]	2720			9.63			
Portland[33]				22.4			$2.927 - 8.262 \times 10^{-3}$
Indiana[37]			7.10 ± 0.60				1.78×10^{-12}
Edwards[37]			15.1 ± 1.1	23.3			6.91×10^{-11}
Indiana[38]				15		21.6×10^{-11}	
RANGE	**1460 - 2720**	**1820 - 2320**	**4.51 - 42**	**9.63 - 50.5**	**520 - 15400**	**21.6×10^{-11}**	**1.78×10^{-12} - 8.262×10^{-3}**

Table 5: Physical properties of sandstone from published literature

SANDSTONES	Density (kg/m^3)	Bulk Density (kg/m^3)	Open Porosity (%)	Porosity (%)	Surface Area (m^2/kg)	Permeability (cm^2)
Brazillian Sandstone - Sample #1[4]				22.6 - 47.28		
Brazillian Sandstone - Sample #2[4]				15.5 - 43.22		
Arkose --- Sample #2[6]						3.81×10^{-10}
Arkose --- Sample #20[6]						4.62×10^{-10}
Arkose --- Sample #22[6]						1.21×10^{-10}
Arkose --- Sample #41[6]						2.49×10^{-10}
Quartz–Arenite[7]		2420	6.40 - 8.57		1750	
Baumberger[8]	2660	2070	22			
Serena (Italy)[9]				5.19		
Mueller[10]				23.90		
Sandstone of Bray[13]				11.2 - 17.1		
Nietulisko[16]	1810		20.6		300	
Villamayor[18]				36.24		
Berea[19]				22		2.96×10^{-9}
Clashach[20]				12.7 - 13.2		
Berea[20]				18.1 - 18.5		
Ohio[20]				14.1 - 14.8		
From Travis Peak, Texas[20]				8.5		
Clashach[20]				15.2		
Beaver[21]				8.4		
Indiana Light[21]				25.7		
Berea[21]				19.5		
Delaware Brownstone[21]				12.8		
Berea[22]				19.7	1230	8.29×10^{-10}
Schilf[24]		2100		16		
Ebenheid[29]			19.6			
Maulbronn[29]			22.2			
Rüthen Green-Sandstone[29]			25.8			
Saal Green-Sandstone[29]			11.5			
Schleerith[29]			16.8			
Ebenheider Red[31]	2660			17.70		
Rüthener Green[31]	2730			25.20		
Berea[33]		2282		21.18		9.87×10^{-10}
Michigan[33]		2362		16.94		
Greenbrae[34]				23.7		$1.46 - 5.19 \times 10^{-2}$
Berea[35]				19.7 - 21.9	840 - 1234	$0.829 - 3.92 \times 10^{-9}$
St. Peter's[35]				17.3	124	9.32×10^{-9}
Indiana Dark[35]				27.5	5000	2.98×10^{-10}
Fontainebleau[38]			11.3 ± 0.7	12.5		5.52×10^{-9}
Bentheimer[38]			11.2 ± 1.2			1.21×10^{-9}
Berea[39]				14		
RANGE	**1810 - 2730**	**2070 - 2420**	**6.4 - 25.8**	**5.19 - 47.28**	**124 - 5000**	**$1.21 \times 10^{-10} - 5.19 \times 10^{-2}$**

MATERIALS

Building materials representative of those commonly used in historic and modern buildings were selected for this investigation. They included; (1) mortar, (2) Indiana limestone, (3) brick, (4) arkose sandstone, (5) Ohio sandstone, and (6) concrete. General index properties, gas permeabilities and saturated hydraulic conductivities of materials 1 through 5 were reported in Ashworth, et al. (2005) (see Appendix A). A concrete specimen was added recently to the test matrix. The index and hydraulic properties have not been determined, nor is the composition of the concrete specimen known. This specimen was added because concrete is one of the commonly used materials in airport terminals. Table 6 summarizes specimen dimensions. Fluorescent salts, water soluble dyes and iodine were used as solutes in various experiments; and water was the solvent.

Table 6: Specimen dimensions

Sample Dimensions

	Height (mm)	Diameter (mm)
Mortar	55.0	71.0
Indiana Limestone	58.5	69.2
Brick	53.9	69.1
Arkose Sandstone	53.0	69.2
Ohio Sandstone	54.8	69.2
Concrete	56.0	75.9

EXPERIMENTAL PROCEDURES AND RESULTS

Three types of laboratory tests were developed for examining contaminant migration within building materials; contact angle, wicking, and migrating dye experiments. Three state-of-the-art characterization techniques were also evaluated. These included X-ray tomography, fluorescent confocal microscopy and gas permeability mapping using an auto-scanning technique. Details of the experimental procedures and results are described below.

Contact Angle Experiments

The contact angle defined as the angle between a drop of liquid (typically water) and a solid surface, is an important property for determining the wetting characteristics of different liquids and the capillary behavior of these fluids within porous materials. Contact angle is

dependent on both the characteristics of the substrate and the fluids in question. It is of great importance for analysis of flow and transport at the microscopic scale.

The standard method for measuring contact angle is to use a smooth material (e.g. glass plate, Teflon coating) for testing. Porous materials or materials with roughness can have a dramatic effect on contact angle measurements. In our case, we wanted to get some preliminary understanding of the behavior of water droplets placed on various samples of building materials, and contact angle enabled these comparisons. The measurements were preformed using a Ramé-Hart Contact Angle Goniometer Model 100-00. The samples were dried prior to the measurements. A ten μL water drop was deposited onto the building material and contact angle was immediately measured using a protractor in the eyepiece. The dry materials quickly absorbed the water drops, thereby requiring an immediate measurement. This was repeated several times at different locations on the surface of each sample. Contact angle was also measured using saturated and blotted building materials to avoid the absorption effect.

For the Ohio sandstone, brick, mortar, and concrete, the drop was instantaneously absorbed into the material and contact angle measurements could not be made on dry materials. This was not surprising and is explained by their high surface areas, small pores, and extremely hydrophilic surfaces. The arkose sandstone and Indiana limestone were not instantaneously absorbed, and the results of the contact angle measurements for these media are shown in Table 2. As expected, the contact angles were all less than 60^o indicating that the drops tended to spread out on the surface rather than beading up (in the case of a drop of water on a waxed car). The results were variable, which also was expected because of the heterogeneity of the material surfaces and pore sizes. The arkose sandstone was quite variable in that sometimes a sessile drop would form and provide ample time to get an accurate reading whereas other times the water was absorbed instantly. The Indiana limestone was the easiest material to measure the contact angle because drops consistently formed and stayed on the surface for an ample amount of time; however even those measurements were wide-ranging. When the specimens were completely saturated, the same problem arose and began to inhibit measurements on the Indiana limestone. The saturated samples of Indiana limestone and arkose sandstone did produce small contact angles ($< 60^o$ indicating that it is more wetting). Although the application of these results is limited, they do provide some useful visual insights into the ability of these materials to take up water samples. These would also be useful for investigating remediation fluids since wetability will be a major factor in determining their efficacy.

Table 7: Measured contact angles on dry and saturated samples

Material	**Range of Contact Angles (°)**			
	Dry		*Saturated*	
	Min.	*Max.*	*Min.*	*Max.*
Indiana Limestone	19	49	14	18
Arkose Sandstone	12	41.5	3	25

Wicking Experiments

One-dimensional wicking experiments were developed as a simple technique for understanding basic macroscopic wicking (imbibition) capabilities of the porous building materials. The experiments were conducted at room temperature (22.5° ± 2°C) with tap water as the migrating fluid in two ways; water introduced at the top of the specimens, and water introduced at the bottom of the specimens. Water temperature was 21°± 1° C. The experimental setup is shown in Figures 1 and 2. Each series of wicking experiments had an identical test setup. The experiments were conducted on oven-dried material specimens individually.

For the test series where water was introduced at the bottom of the specimens (wicking test series I), the samples were placed in a plexiglass box (Figure 1). This box consisted of a notch that facilitated a constant water level 5 mm above the bottom of the specimens. All specimens were marked with a thin permanent marker at 5 mm intervals along their heights, as shown in Figure 3. The movement of water through the specimens was continuously monitored using a digital camcorder until the water movement stopped as determined by visual inspection. Total recording time for both test series varied from about 25 min to 2,747 min, depending on the type of the material.

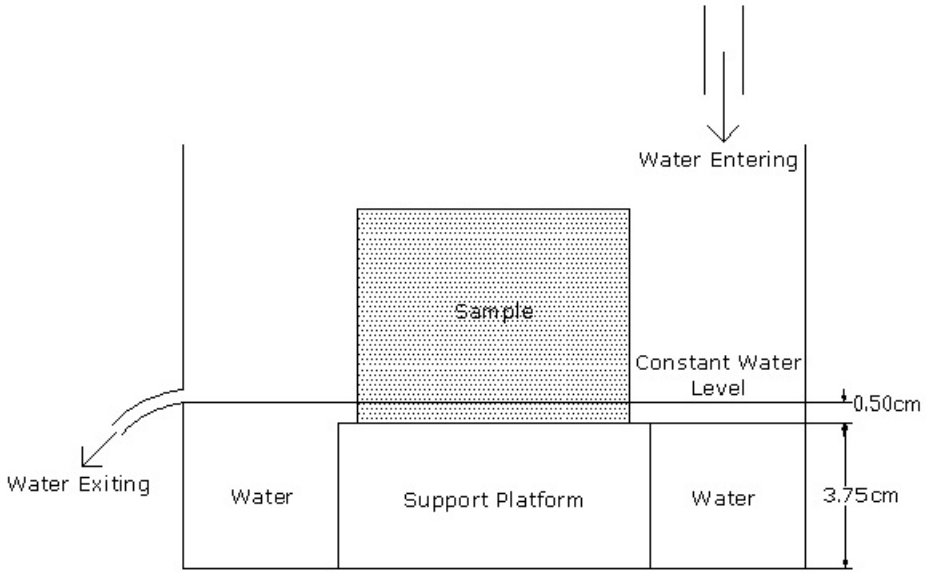

Figure 1: Schematic of the wicking test series I setup (not to scale)

In the second series of experiments, the water was introduced at the top of the sample. The sample was oven dried, and its orientation was switched from the first test series, so that the water entered the specimen from the same face as in the first test. The experimental setup is depicted in Figure 2. A plexiglass cylinder was placed on top of the specimen. The inside diameter of the plexiglass cylinder was almost the same as the diameter of the specimens, except in the case of the concrete specimen. A waterproof silicone sealant was used at the contact between the plexiglass cylinder and the specimen to prevent any leakage. The plexiglass cylinder consisted of a notch, which facilitated in maintaining a constant water level of 4 cm above the top of the specimens. As in the first test, the samples had markings at 5 mm intervals and the test was continuously recorded using a digital camcorder.

Still pictures of the specimens (an example is shown in Figure 3) were obtained at 5 minute intervals from the digital recordings. This allowed us to determine the water level at a particular time interval. The water level was measured at the centerline through the markings. The water level was not always perfectly horizontal due to the intrinsic heterogeneities within each specimen. The amount of water taken up by each specimen was determined by weight.

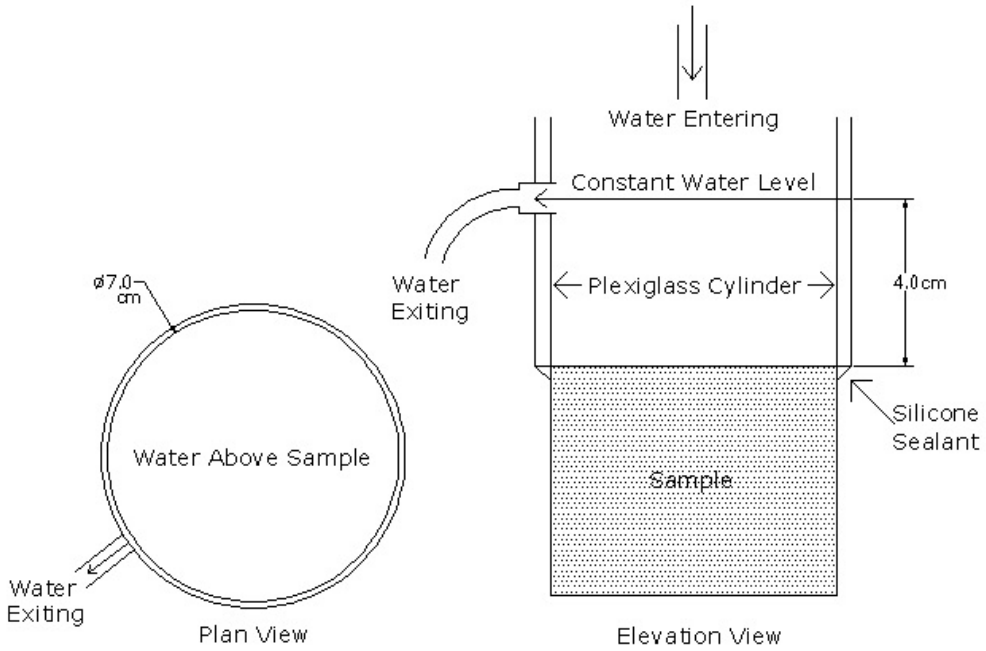

Figure 2: Schematic of wicking test series II setup (not to scale)

Figure 3: Ohio sandstone during wicking test series II

In the first test series when water was introduced from the bottom of the specimens, the initial water level at time zero was at 5 mm above the bottom of the specimens. The rate of water imbibition was calculated for a particular time by dividing the difference in the water levels for the current and the previous time intervals by the time interval, which was generally 5 minutes. Water did not reach the top of the arkose sandstone and Indiana limestone specimens during the

investigation time period. All results from these test series are plotted using the symbol, solid diamond.

In the second test series when water was introduced from the top of the specimens, the water level above the top of the specimen was maintained at 4 cm. Time "zero" in this experiment was considered when the water level reached the first 5 mm mark, down from the top of the specimen. The height of the water level was again determined at five minute intervals. The rates of imbibition were again calculated the same way. Again, the water did not migrate to the bottom of the arkose sandstone; however, in the second test series it traveled through the Indiana limestone specimen. All test results are plotted using the symbol, solid circle. It should be noted that given the design of this second test, 4 cm of water head was applied to the samples. This could have helped facilitate some additional movement of the fluid; although, it was barely discernable in the results and not statistically significant.

Results are shown in Figures 4 through 9 and plotted in the following format. For each specimen, the plot on the left shows water level versus time for the data from the two test series. The plot on the right shows the rate of imbibition versus time. To facilitate direct comparisons, all y axes are on the same scale, and x-axes are presented for up to 80 minutes. In cases where measurements were made for longer time periods (e.g. Figures 5 and 7) a separate set of plots with the longer time scales is also provided. In addition, short horizontal lines are added in the plots to indicate the final water levels reached at the end of the test, if the measurements were made beyond 80 minutes. These experiments are easy to conduct and could be used to develop a data base on building material imbibition rates and variability.

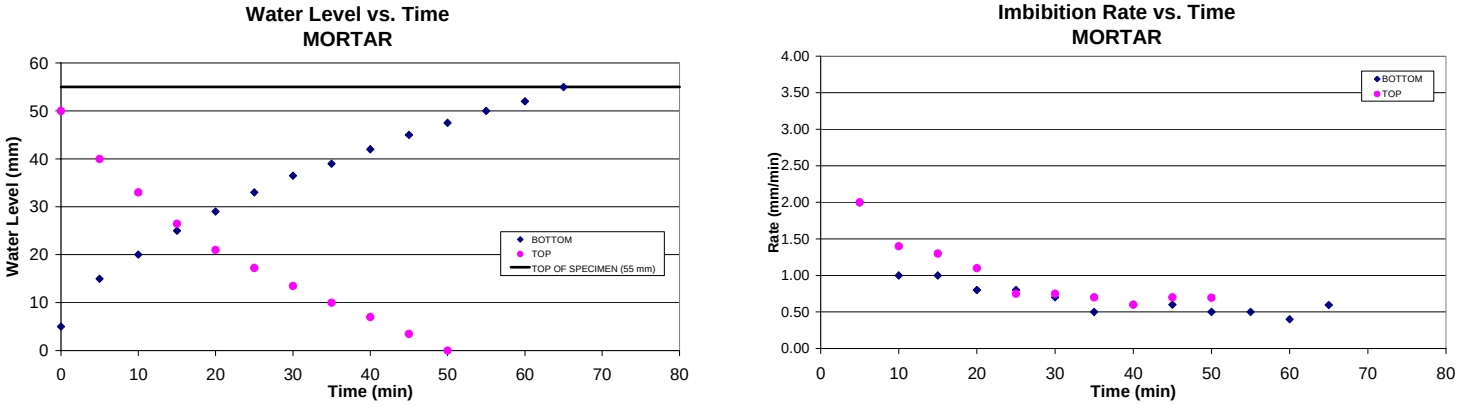

Figure 4: Wicking test results of mortar specimen

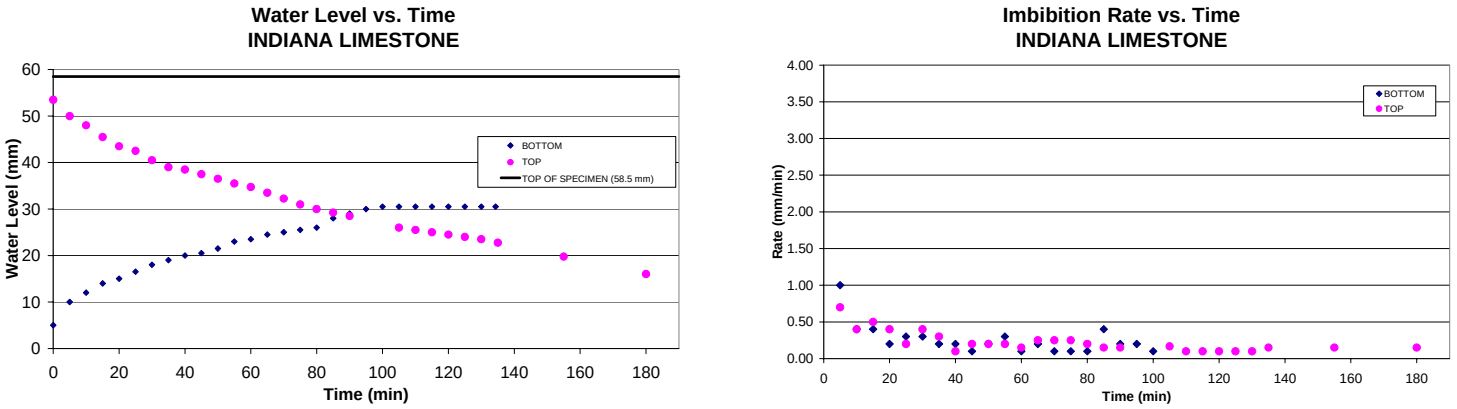

(a) Up to 190 minutes

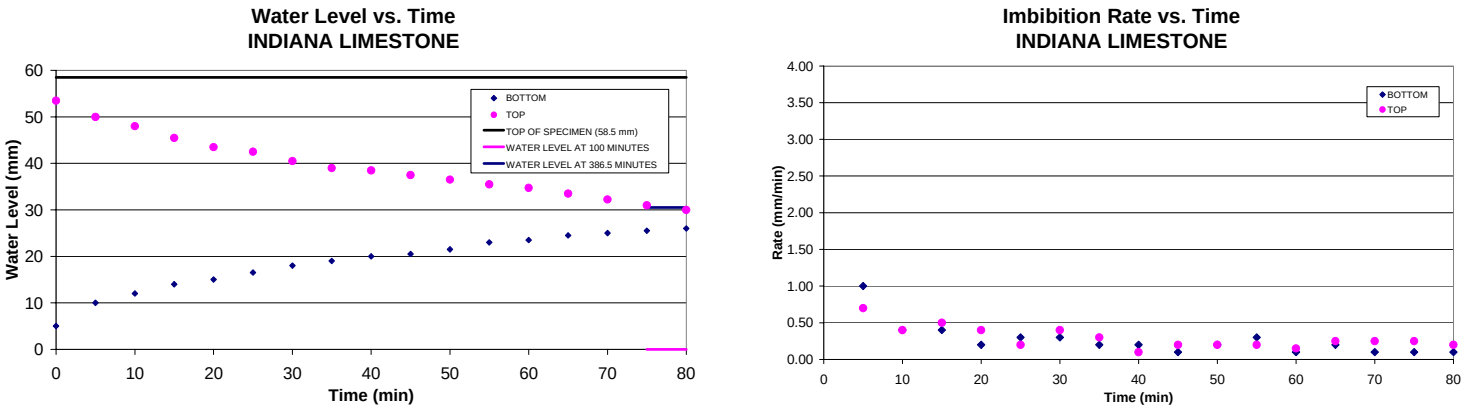

(b) Up to 80 minutes

Figure 5: Wicking test results of Indiana limestone specimen

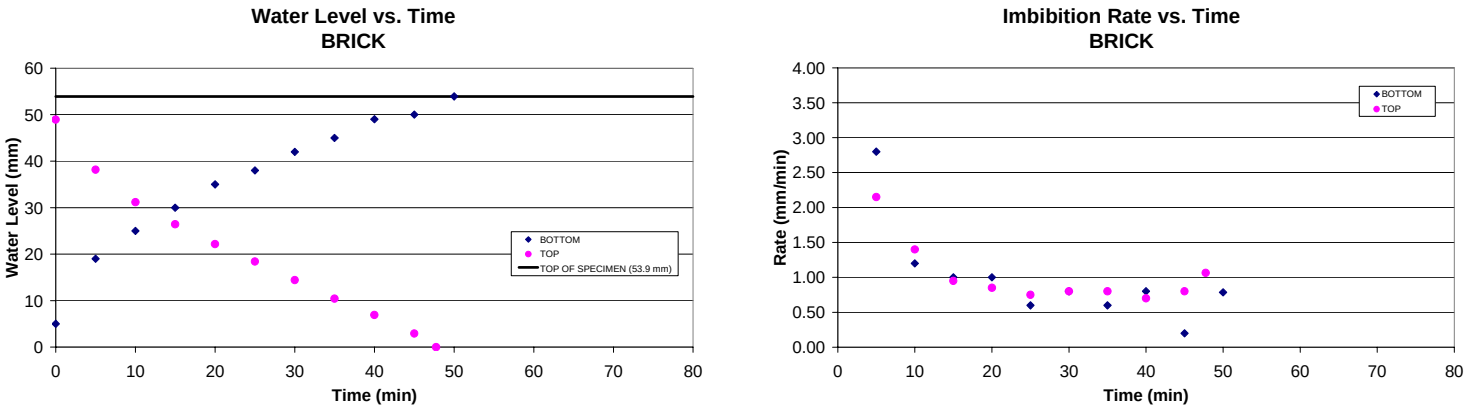

Figure 6: Wicking test results of brick specimen

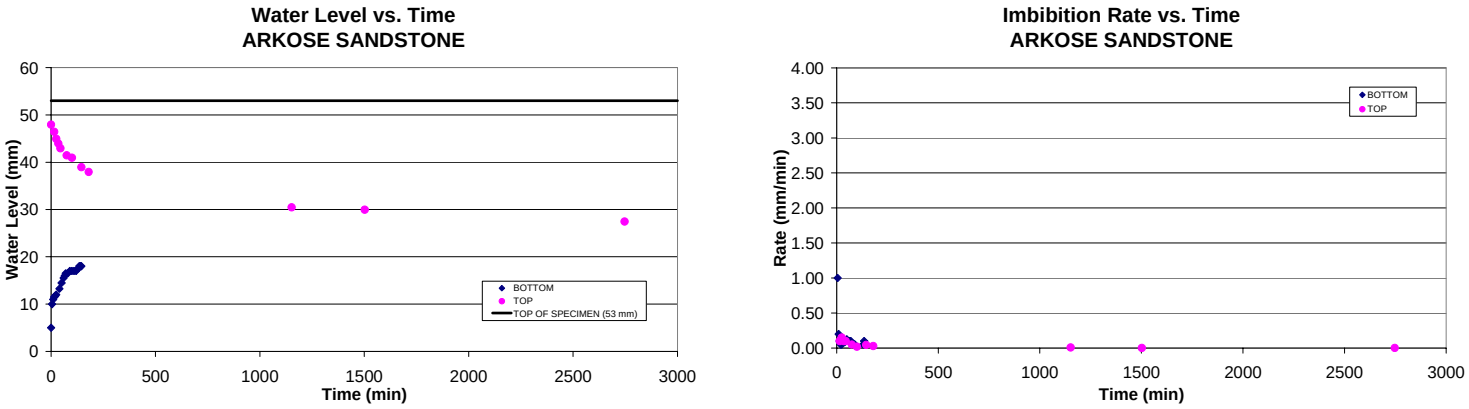

(a) Up to 3000 minutes

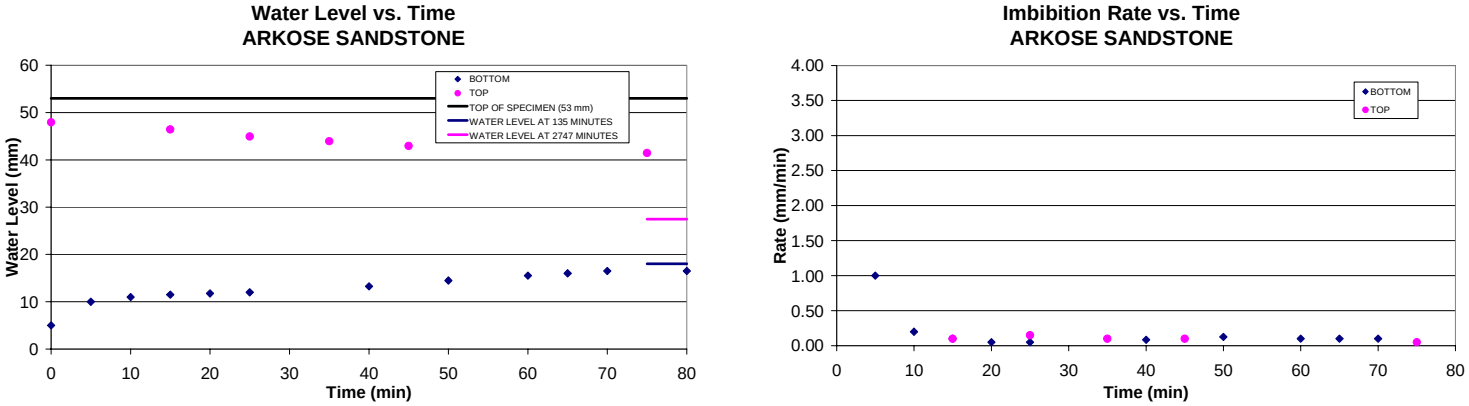

(b) Up to 80 minutes

Figure 7: Wicking test results of arkose sandstone specimen

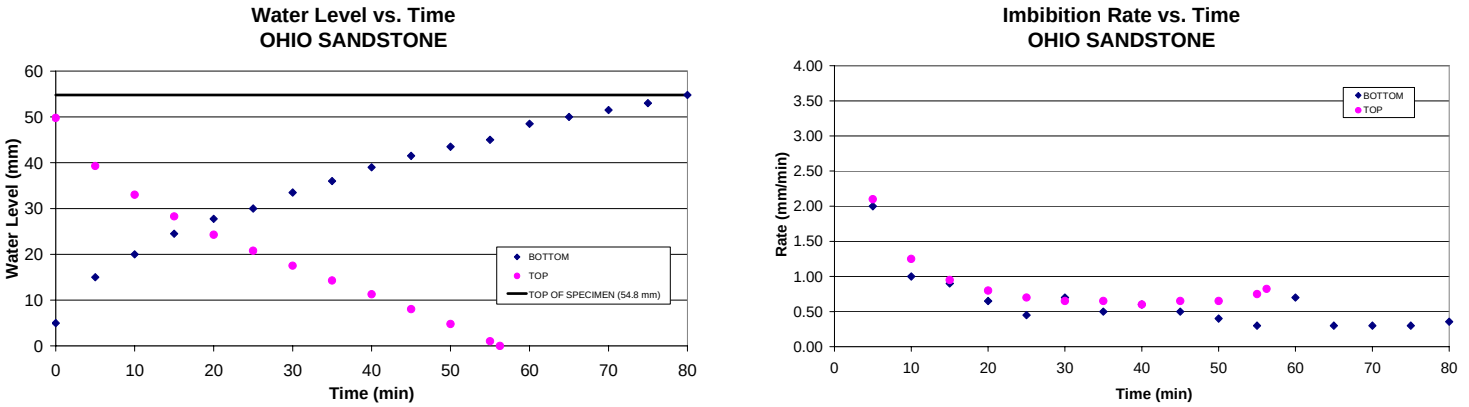

Figure 8: Wicking test results of Ohio sandstone specimen

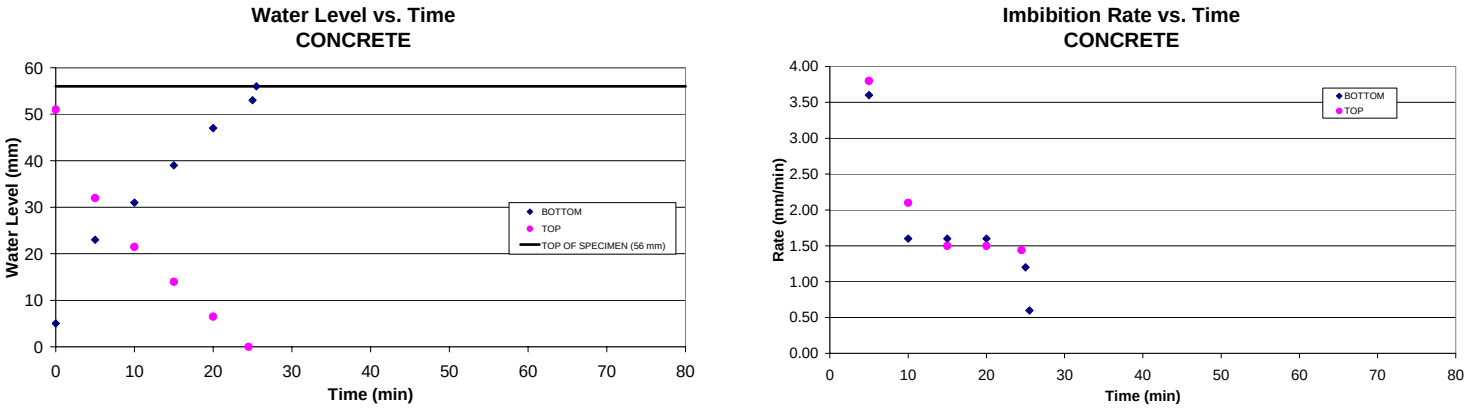

Figure 9: Wicking test results of concrete specimen

Dye Migration Experiment

The dye migration experiments provided another example of visualizing fluid transport; however, in this case, a two-dimensional physical micromodel was used. The micromodel consists of a thin layer (about 0.6 mm thick) of dry sand/clay media sandwiched between two glass plates and sealed from all sides (Figure 10a). Two needles were used for an inlet and outlet. The glass plates were approximately 2.5 cm by 7.5 cm. The media consisted of Ottawa sand mixed with a small amount of kaolinite clay (2 percent by weight). The total porosity of the glass slide was known (about 35%) but the porosity at any given location was not known due to packing heterogeneity. Water-soluble green dye was diluted with distilled water in a 15:1 ratio by volume. The solution was put into a syringe and attached to the needle on the left. The green dye solution was slowly fed into the micromodel at a rate of 0.05 mL every 30 seconds for a total of 5.5 min. The whole process was video recorded so that the path of travel could be analyzed.

Still pictures were captured at the beginning of each dose as shown in Figure 10. Although the last (11^{th}) dose was administered at approximately 5 minutes, the video was recorded was done for up to 20 minutes from the beginning of the test. Images captured between 6 and 20 minutes are shown in Figure 11. Note that the dye continued to move at the front due to imbibition into the dry sand/clay media. The syringe had a beveled tip that may have resulted in the initial movement of the dye upward. However, even after an initial front was established (after 4 minutes) it is clear that there are some instabilities in the front due to the slightly heterogeneous nature of the packing. The front continues to move with some instabilities and fingering visible. The still pictures show that after the final dose was introduced, the dyed solution continued to move through imbibition until the sixteenth minute and then ceased.

These micromodel experiments can be conducted using a variety of media and operating conditions to better understand heterogenous media. In addition, the micromodels can be observed under a microscope to determine pore characteristics and effects on contaminant migration.

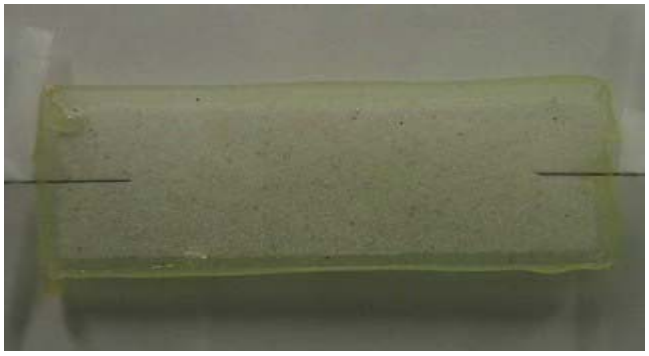

(a) Initial

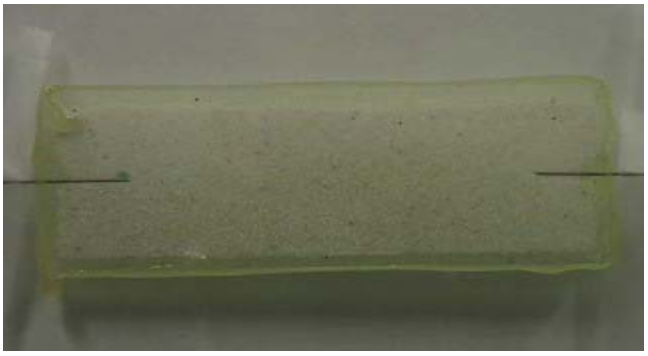

(b) Dose 1 (0 min)

(c) Dose 2 (0.5 min)

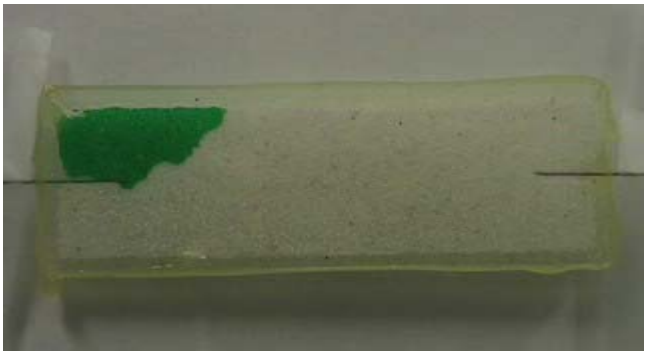

(d) Dose 3 (1 min)

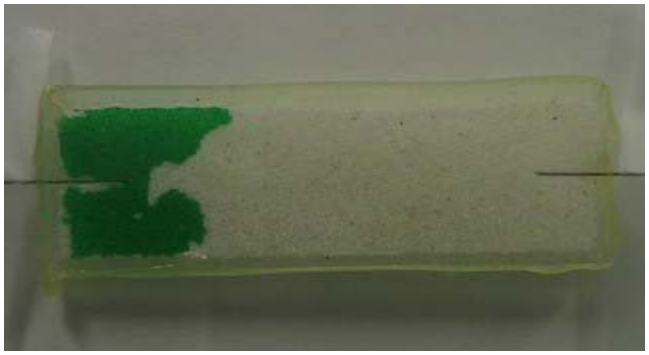

(e) Dose 4 (1.5 min)

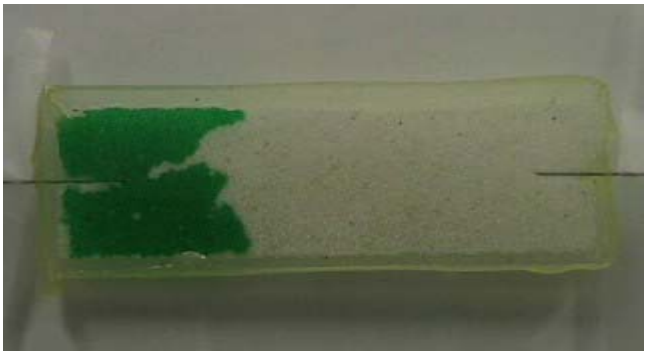

(f) Dose 5 (2 min)

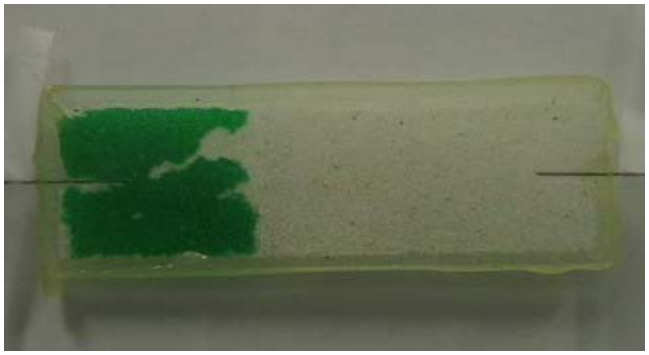

(g) Dose 6 (2.5 min)

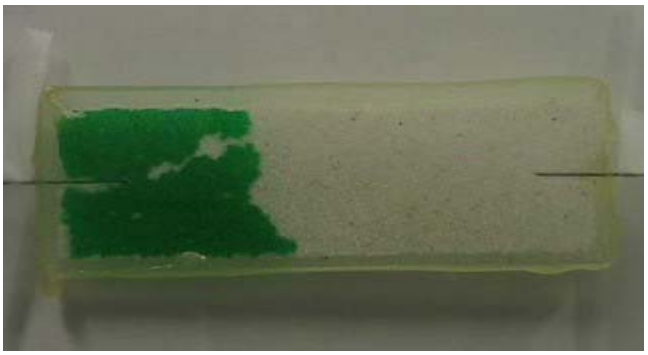

(h) Dose 7 (3 min)

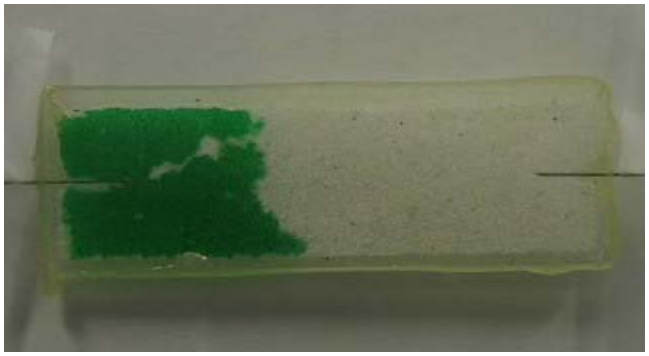

(i) Dose 8 (3.5 min)

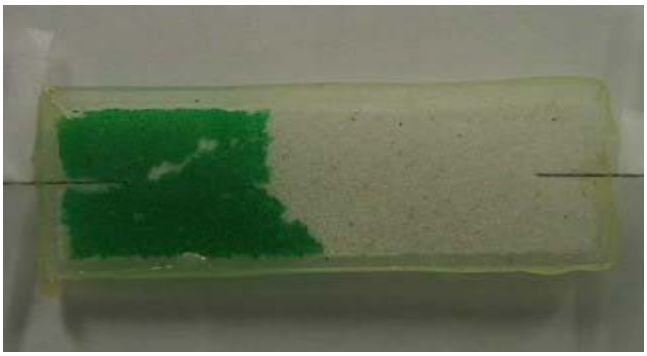

(j) Dose 9 (4 min)

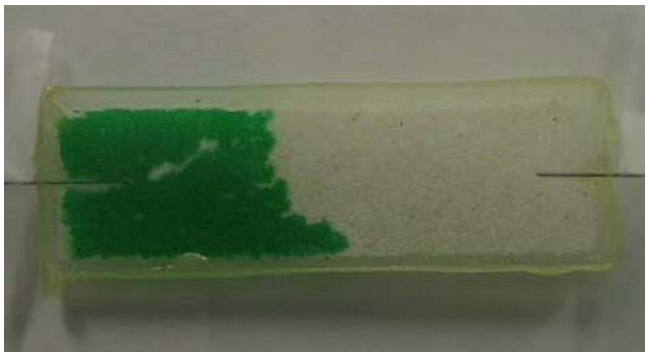

(k) Dose 10 (4.5 min)

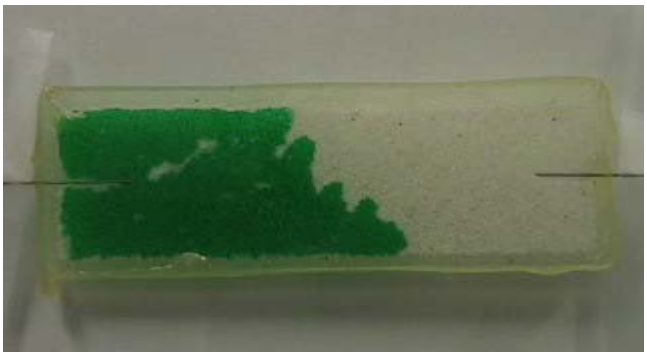

(l) Dose 11 (5 min)

Figure 10: Dye position at the beginning of dose

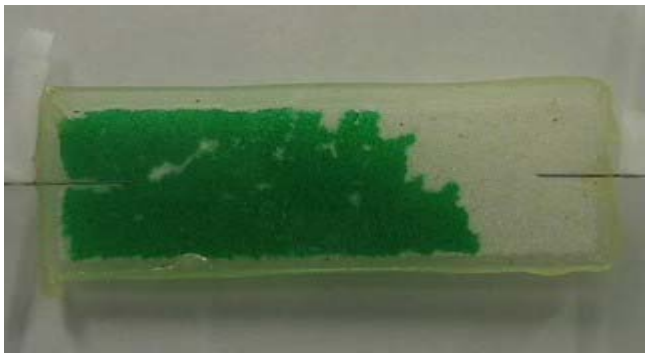

(a) 6 minutes

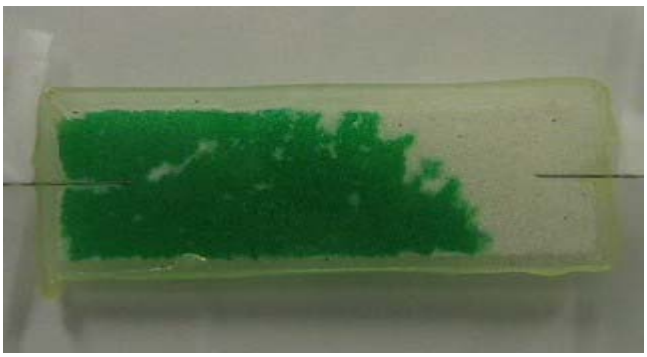

(b) 7 minutes

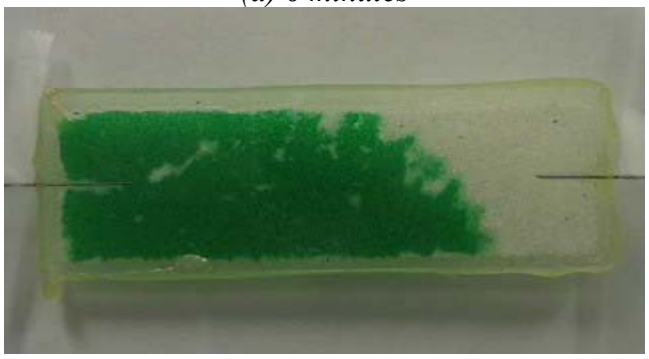

(c) 8 minutes

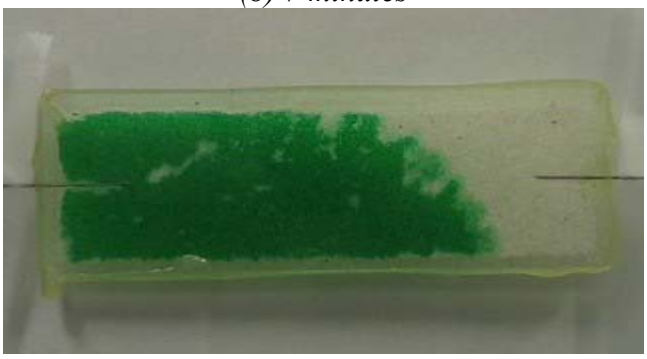

(d) 9 minutes

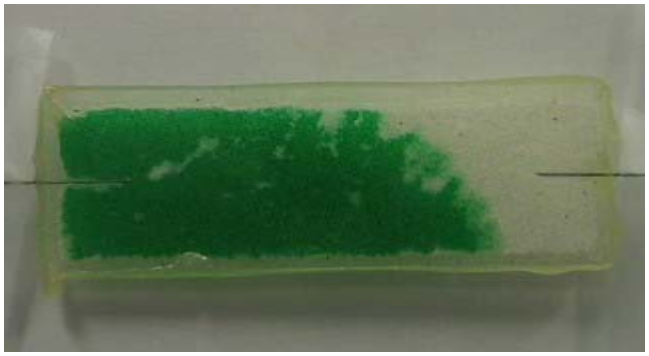

(e) 10 minutes

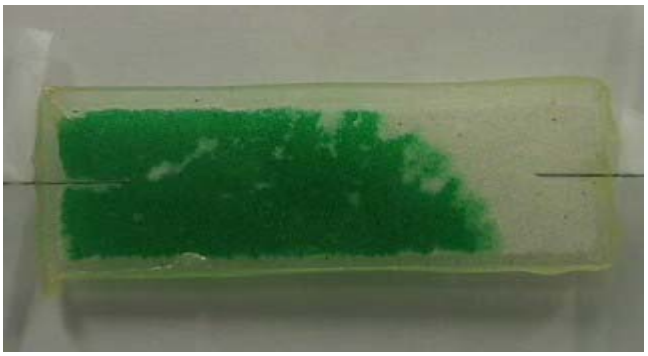

(f) 11 minutes

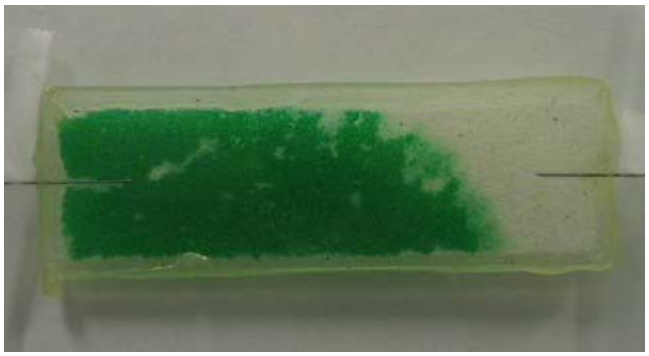

(g) 12 minutes

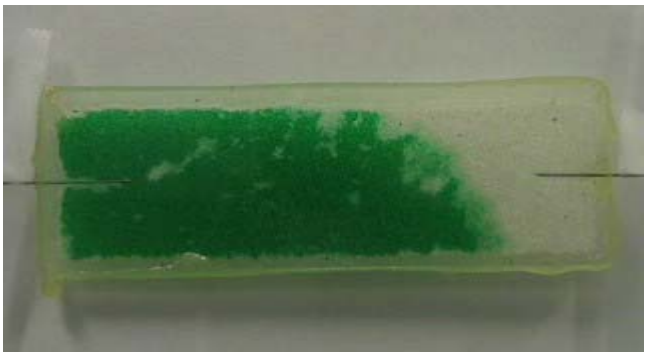

(h) 13 minutes

(i) 14 minutes

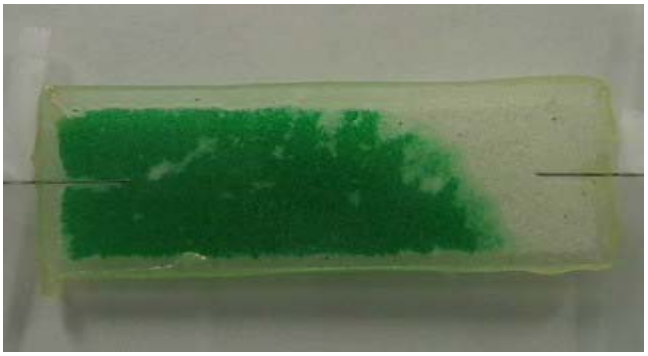

(j) 15 minutes

(k) 16 minutes

(l) 17 minutes

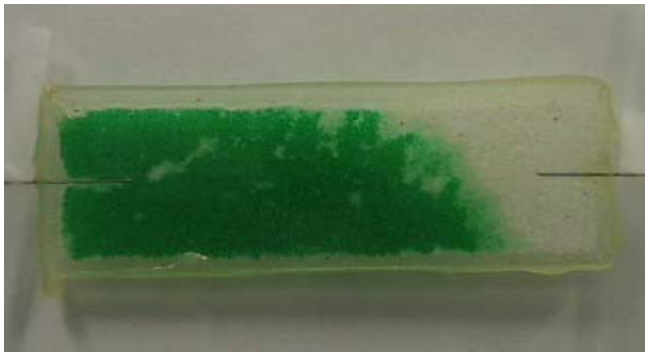

(m) 18 minutes

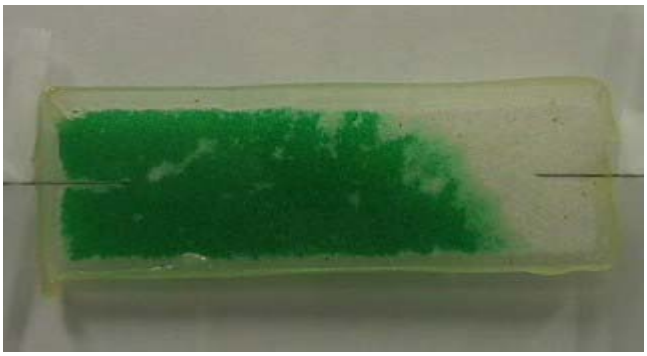

(n) 19 minutes

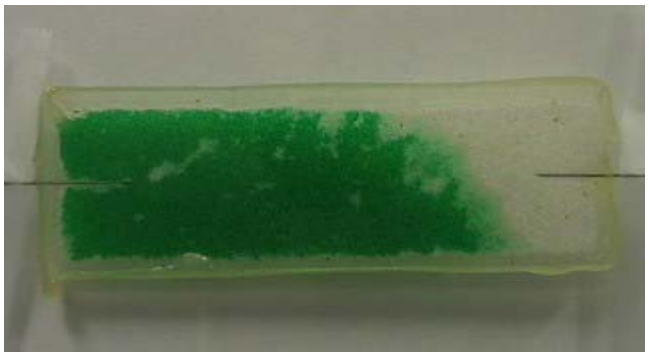

(o) 20 minutes

Figure 11: Dye position at given time

CT Scanning

X-ray micro-computer tomography was explored as a technique to assist in quantifying details of geomorphic pore structures of building materials. This information would be very relevant to microscopic and macroscopic modeling of fluid transport in porous media.

Samples of Ohio sandstone and concrete were sent to Prof. Whitey Hagadorn, at Amherst College in Massachusetts for X-ray scanning after it was determined that the CT scanner at UVM was not powerful enough to scan high density building materials. The scanner at Amherst College is shown in Figure 12. It is a microfocus X-ray CT scanner, made by Skyscan, model number 1172. It has a 100 keV source, and a 10 megapixel CCD, with spatial resolution approaching 0.6 x 0.6 x 0.6 microns per voxel dimension. The specimens were scanned at 50 keV and 200 uA, using a 0.5 mm thick Al filter, and were scanned through 180 degrees of rotation with projection images collected every 0.1 or 0.3 degrees of rotation. Reconstructed images were generated using a modified filtered backprojection algorithm, and contrast thresholding performed such that air surrounding the sample was normalized to a grayscale value of zero.

The distance between scans on the specimen is 1.51 μm. An example scan of Ohio sandstone is shown in Figure 13, where the individual grains can be seen. The color of the grains varies from white to dark gray. The black spaces within the specimen are the pore spaces.

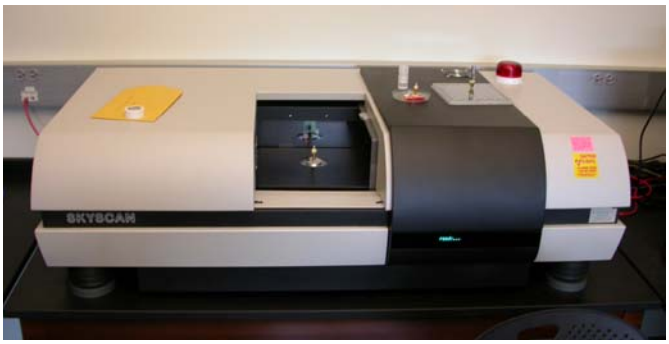

(a) Photograph of microfocus X-ray CT scanner used in this study

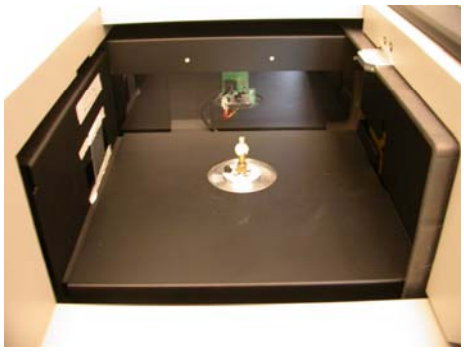

(b) photograph of the inside of the scanner with specimen mounted in the center

Figure 12: X-ray CT scanner used in this study

A Matlab image analysis program was used to crop the original image for convenience to get a representative section to analyze further, as shown in Figure 14. The cropped image was about 3.5 mm x 3.5 mm in size. The cropped image was turned into a black and white image using our best estimate of the appropriate gray scale threshold to differentiate between pore space and grains, as shown in Figure 15. This manipulated image shows that the shape and size of the pores can vary greatly throughout the specimen. The image was reassigned to a matrix of ones and zeros corresponding to white and black pixels, respectively. The white pixels represent pore space and the black pixels are the grains. The porosity calculation is then simple arithmetic using the matrix created. The calculated porosity for this specific slice of Ohio sandstone was about 0.173.

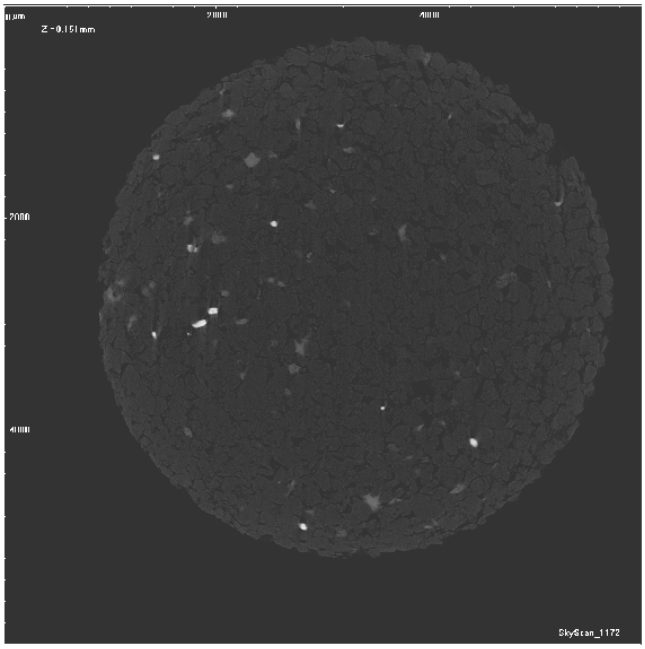

Figure 13: Original scanned image of a 5 mm diameter Ohio sandstone specimen

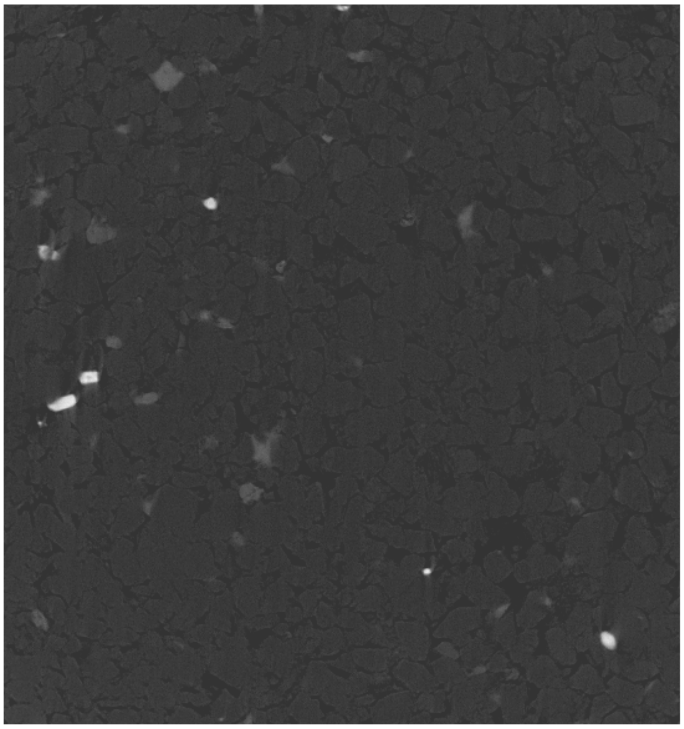

Figure 14: Cropped image of the original scan of Figure 13

Figure 15: Filtered image of Figure 14

Another 5 mm diameter core of the Ohio sandstone was obtained and scanned in the CT scanner. To assess the variability in the porosity of the specimen, we analyzed every 75th slice of the scans. The results are presented in Figure 16. Similar to Figures 14 and 15, image of a cropped scan and corresponding filtered image are presented. The distance between two of the two consecutive scans presented in Figure 16 is 0.1125 mm. Corresponding porosities are summarized in Table 8. As evident from Figure 16 and Table 8, the pore structure and porosity vary significantly over distances as short as 0.1125 mm.

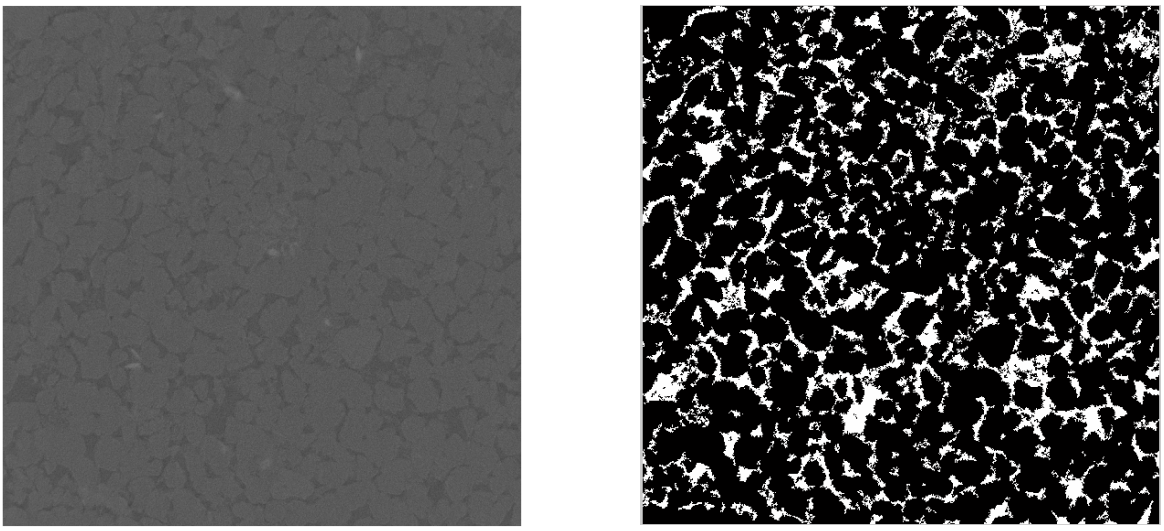

(a) Scan cropped and filtered image of Slice 1

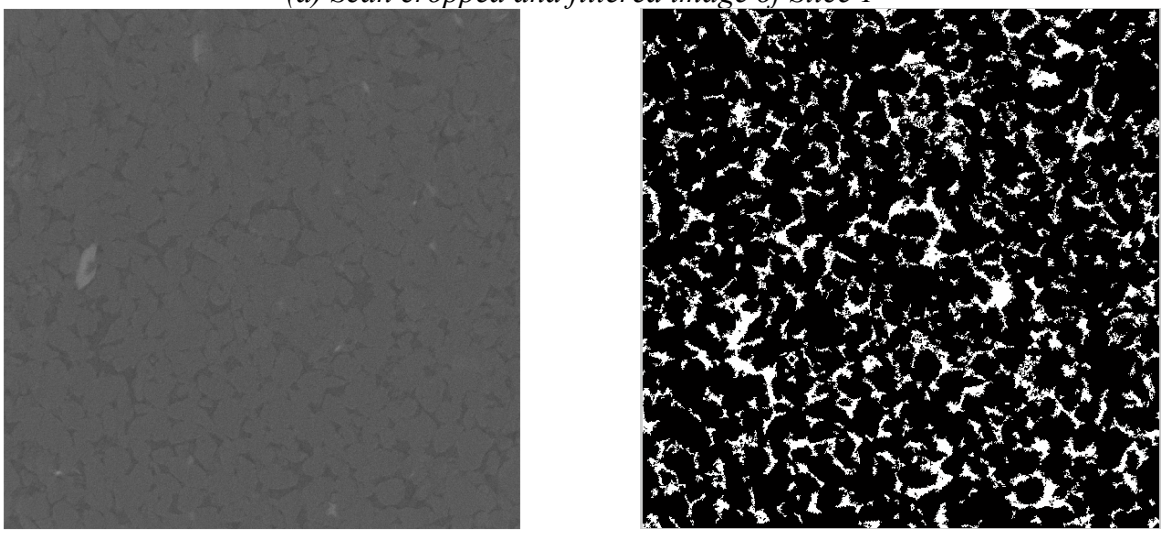

(b) Scan cropped and filtered image of Slice 2

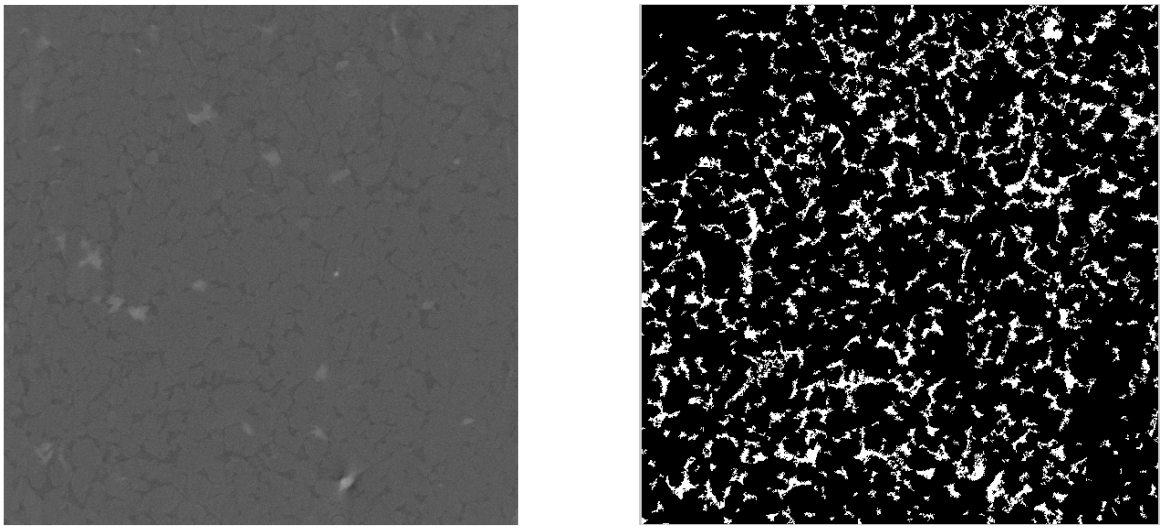

(c) Scan cropped and filtered image of Slice 3

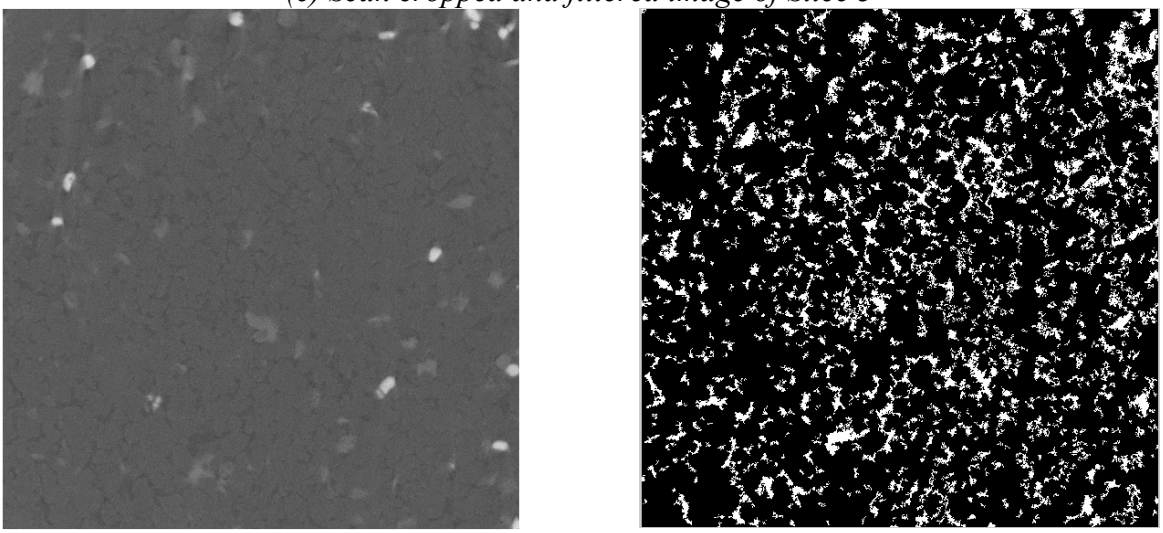

(d) Scan cropped and filtered image of Slice 4

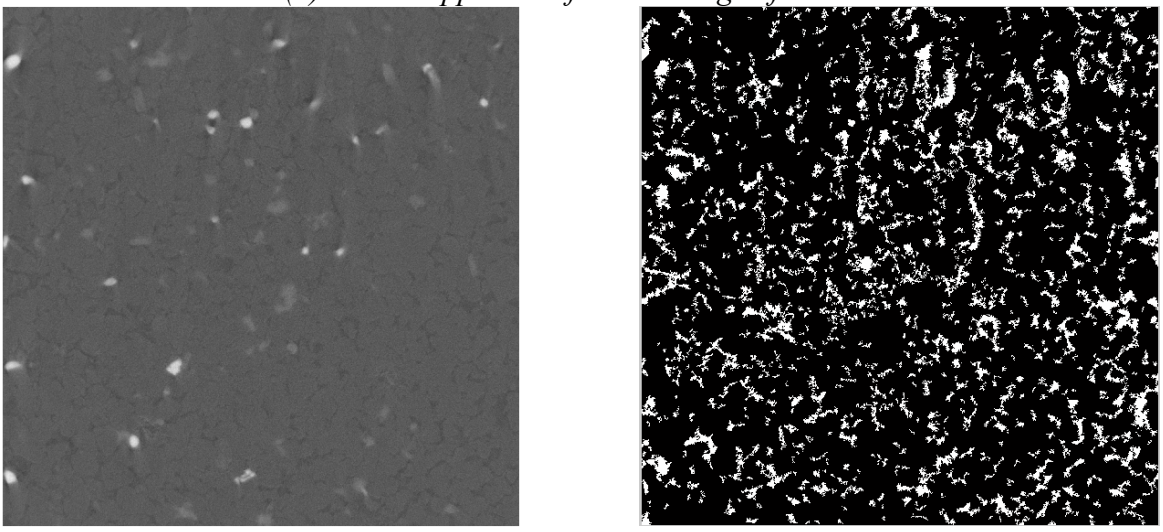

(e) Scan cropped and filtered image of Slice 5

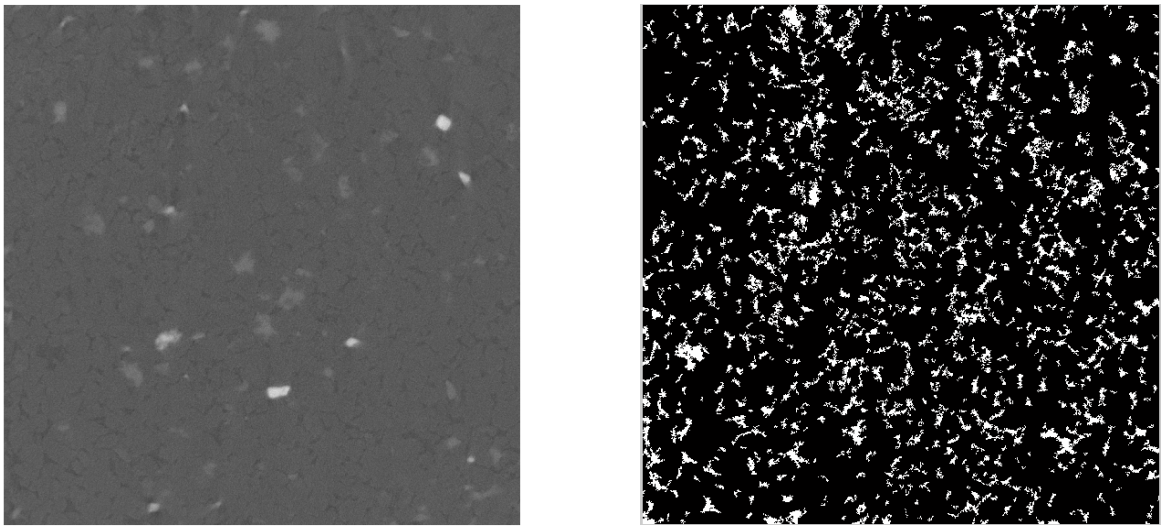

(f) Scan cropped and filtered image of Slice 6

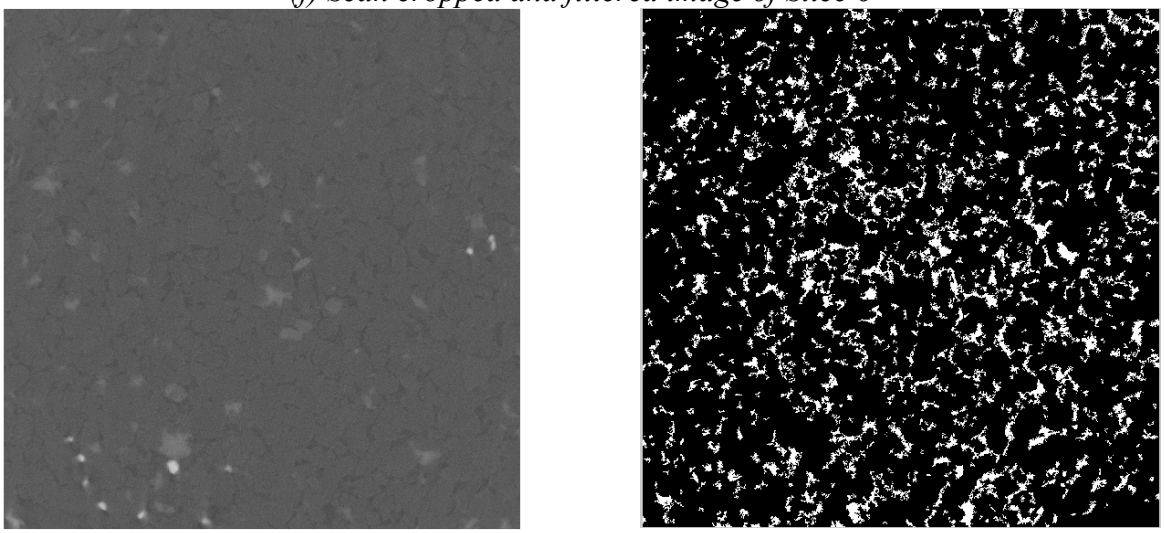

(g) Scan cropped and filtered image of Slice 7

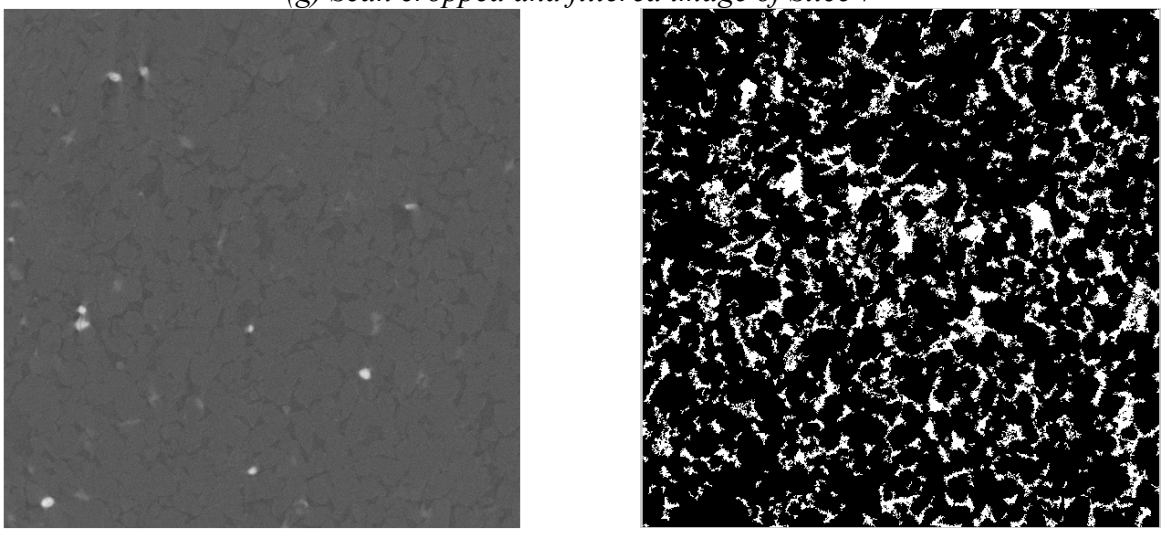

(h) Scan cropped and filtered image of Slice 8

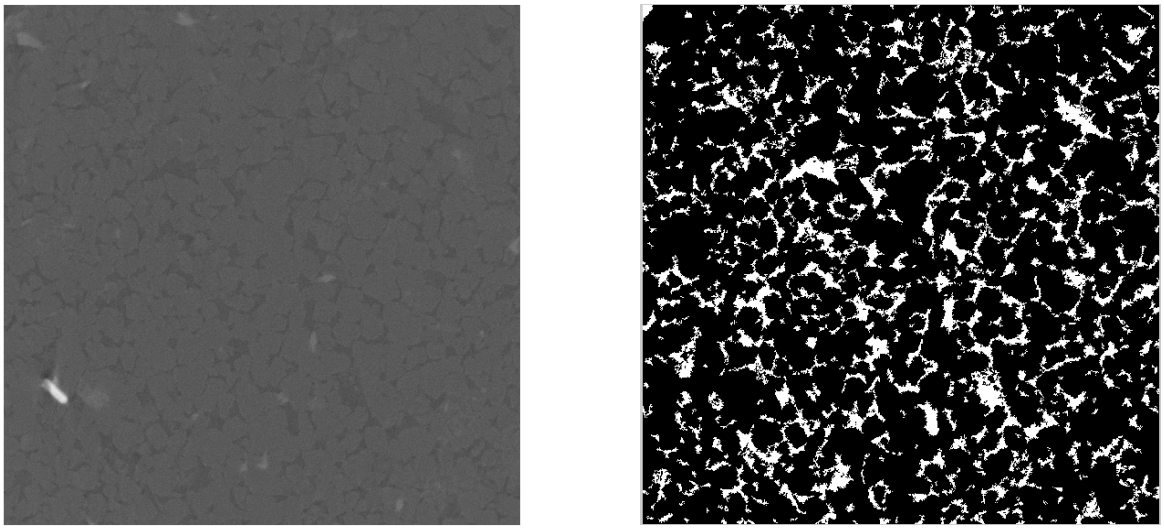

(i) Scan cropped and filtered image of Slice 9

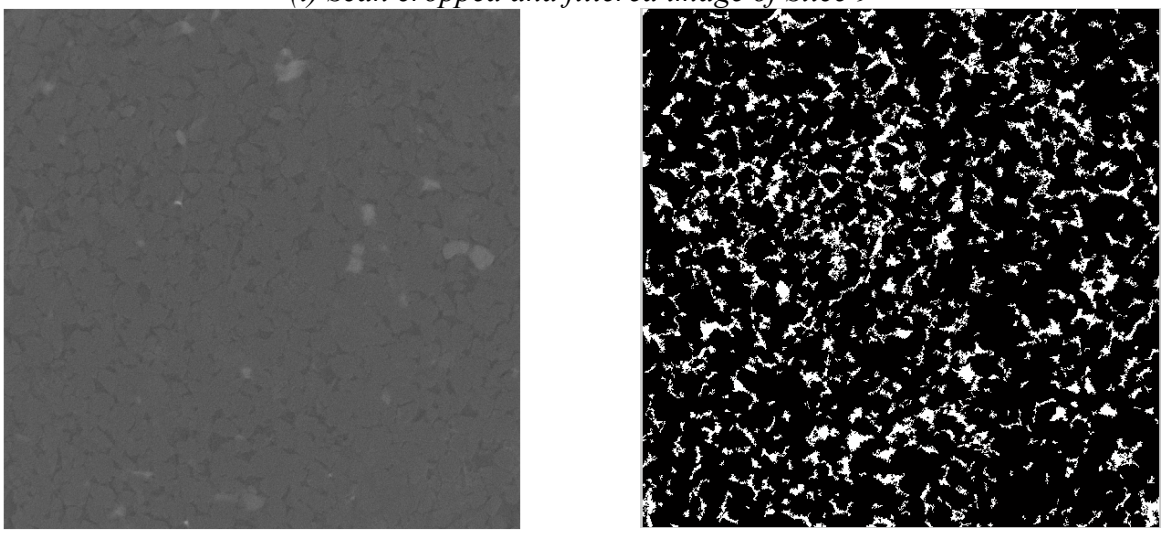

(j) Scan cropped and filtered image of Slice 10

Figure 16: Scans (cropped and filtered images) for 10 slices of Ohio Sandstone separated by a distance of 0.1125 mm

Pieces of concrete were also scanned. The concrete specimen was quite brittle and a 5 mm diameter uniform core of concrete could not be obtained. Therefore, the piece of concrete scanned was of arbitrary shape. About 21 drops of iodine solution (diluted in water) were dropped on the piece of concrete as shown in Figure 17. The X-ray scans were obtained before and after introducing iodine solution without removing the specimen from its location. Example scans (before and after) are shown in Figure 18. Both scans are for the same slice. As shown in Figure 18b, the iodine residue (following evaporation) is clearly observed along the edges of the specimen and inside some pores.

CT scanning provides an excellent tool for quantifying and visualizing pore sizes and porosity. This technique coupled with previous methods could provide more insight into contaminant migration and subsequent remediation from building materials.

Table 8: Porosities determined through image analysis for scans presented in Figure 16

Slice Number	Porosity
1	0.186
2	0.156
3	0.129
4	0.144
5	0.131
6	0.112
7	0.124
8	0.157
9	0.159
10	0.137

Figure 17: Concrete specimen imbibed with 21 drops of iodine solution

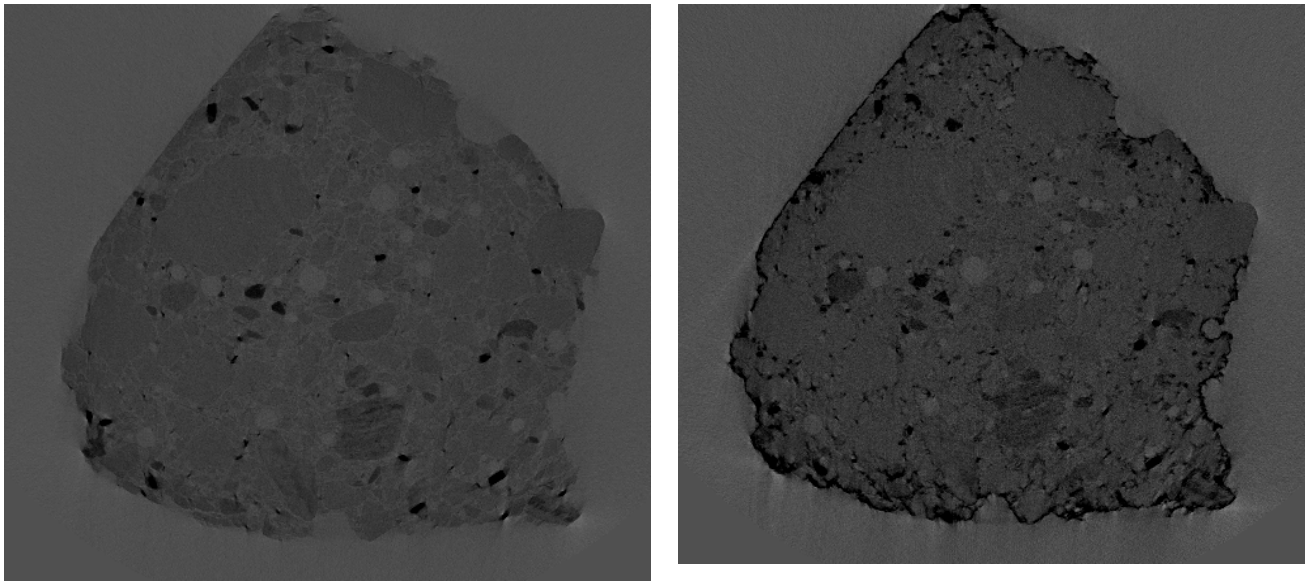

(a) X-ray scan before introducing iodine solution *(b) X-ray scan after introducing 21 drops of iodine solution*

Figure 18: X-ray CT scans of the concrete specimen before and after introducing iodine solution

Fluorescent Confocal Microscopy

A fluorescent confocal microscope was used to quantify individual pore sizes at and near the surface of the rock. The confocal microscope can take images to about a 0.2 mm depth. A fluorescein sodium salt solution (0.04% by mass) was imbibed by a piece of Indiana limestone (about 2.5 mm thickness) overnight. The surface pore structure of this specimen was then captured using a ***Zeiss*** LSM 510 META Confocal Laser Scanning Imaging System with a magnification of 10x. The green spaces represent the pores as the confocal microscope detects the fluorescing dye-filled pores.

The ***Zeiss*** LSM Imaging software allows one to perform various functions such as measuring pore dimensions, as well as animate the surface of the specimen and examine three dimensional views (Figures 19 and 20). The pore radii measured in the Indiana limestone ranged from approximately 7 to 265 μm; however, smaller pores were also present. Measuring those smaller pores becomes increasingly difficult as the resolution is diminished. Pore shape also varied; however, a circular-type pore was the most prominent.

Figure 21 shows the same image as Figure 19; however, it is manipulated to show the depths of individual pores. It was noted that the largest pores in this rock sample were typically the deepest. Fluorescent confocal microscopy offers a wide range of applications to further study contaminant transport in porous building materials. Coupled with the micromodels or thin rock sections, specific fluorescing contaminants could be traced before and after cleanup applications to determine the efficacy of removal.

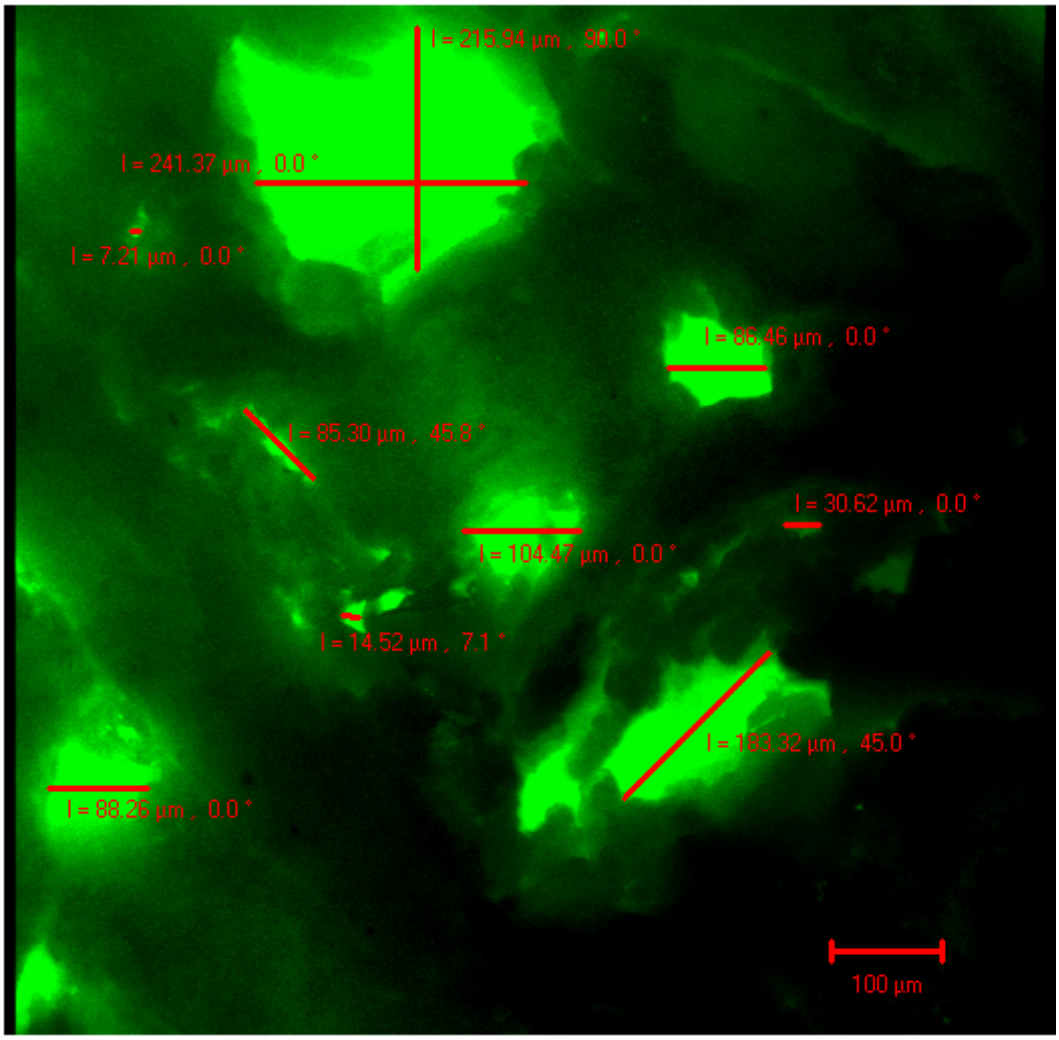

Figure 19: XY axis rotation snap shot with dimensions at 10x magnification (Indiana limestone)

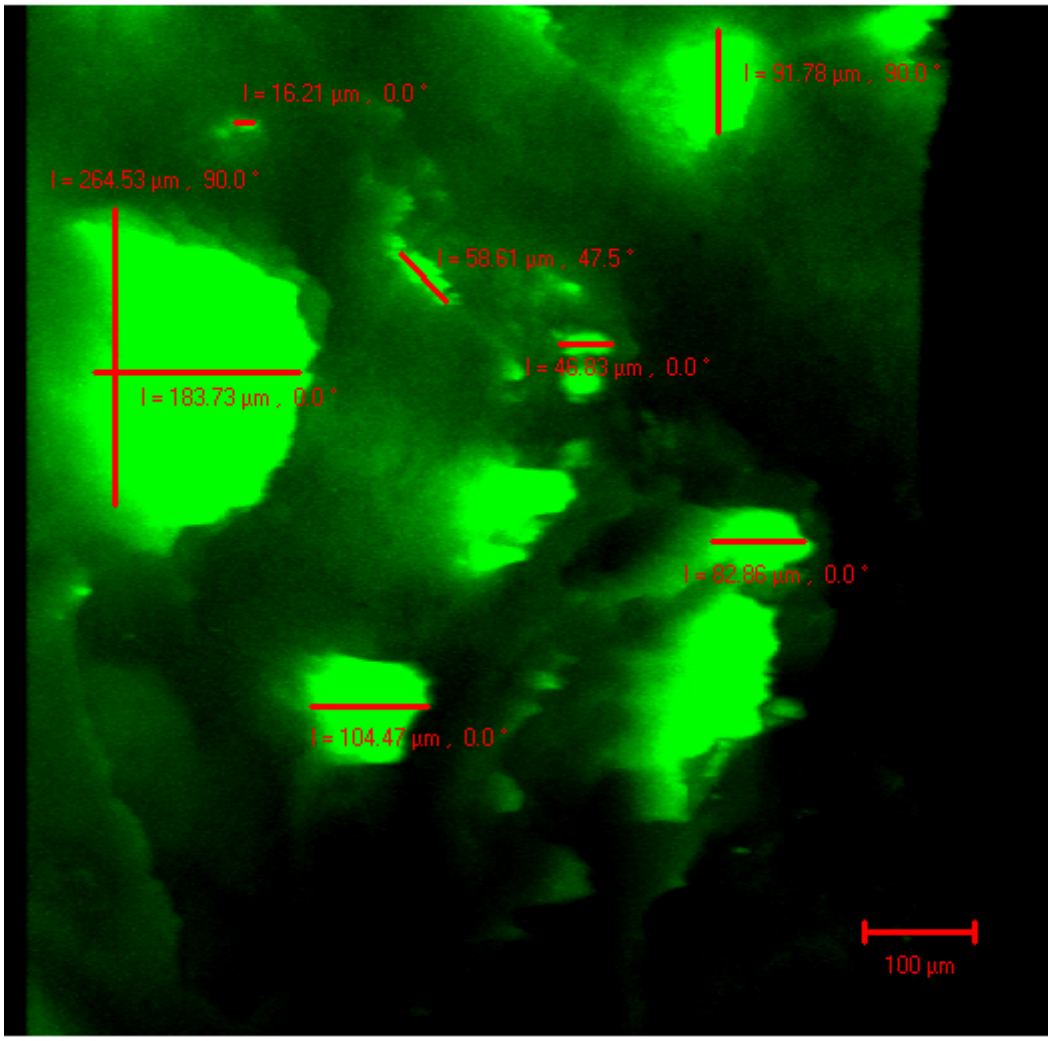

Figure 20: XX axis rotation snap shot with dimensions at 10x magnification (Indiana limestone)

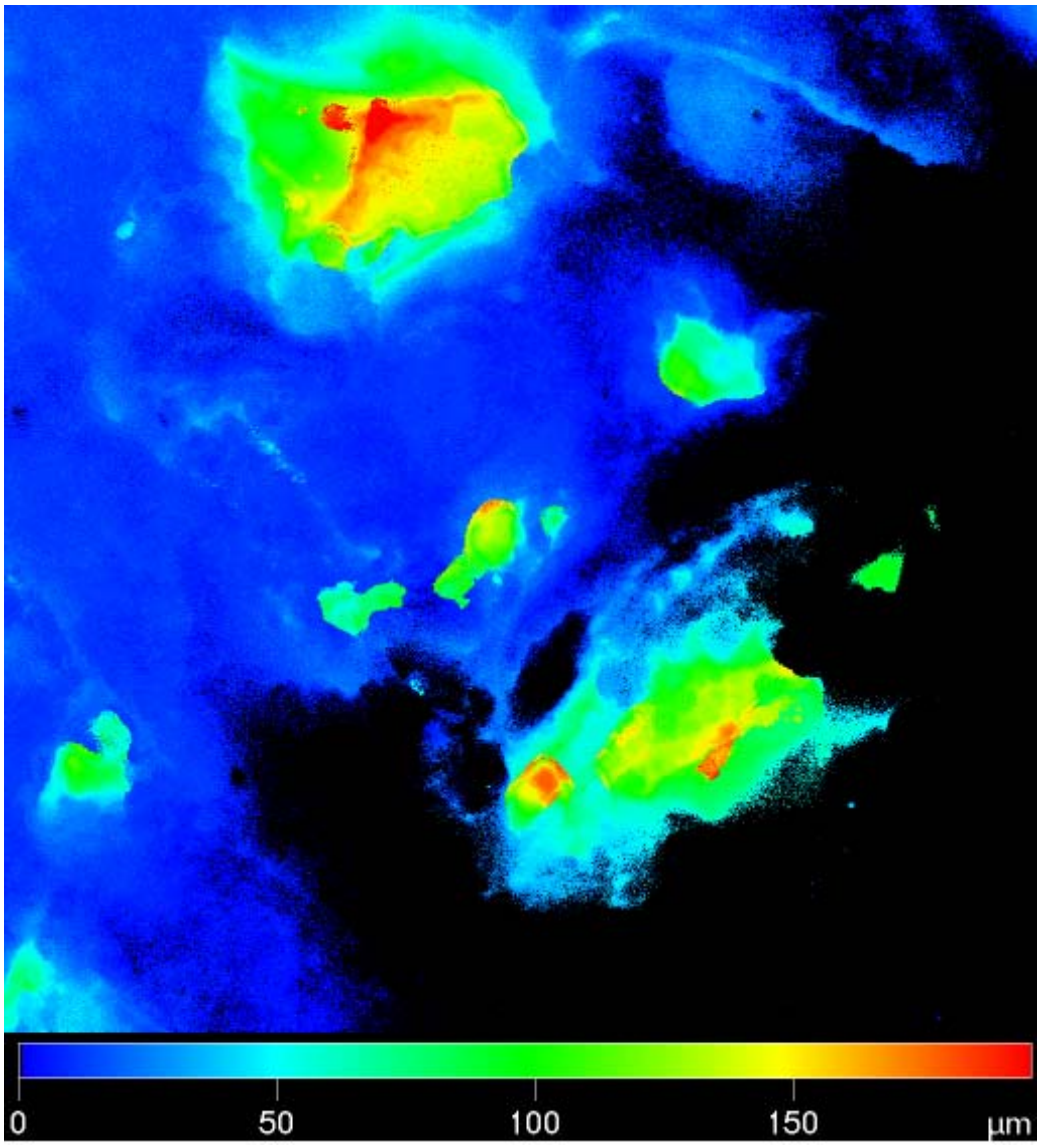

Figure 21: Depth Coding at 10x magnification of image shown in Figure 1

Gas Permeability Mapping Using an "Autoscan"

This new technique of mapping air permeability at the surface of a porous material was used to evaluate the inherent heterogeneity in building materials that have an appearance of being homogeneous. For this purpose, the *AutoScan II* core scanner system, developed by New England Research, Inc., was used. This system allows the user to collect spatially integrated measurements of gas permeability, complex electrical impedance, and ultrasonic compressional and shear velocities on slabbed core and large rock surfaces.

The AutoScan II equipment allows the specimen to be oriented on an x-y grid by a computer to make measurements at specified locations. The spacing between measurements can be as small as 0.1 mm. The permeability is measured using a gas injection technique. The equipment also allows measurements of ultrasonic velocities and electrical resistivity; however, only gas permeability was measured for this study.

A permeameter probe is pressed against the surface of the specimen. Pressurized gas (typically nitrogen) flows through an aperture into the specimen. The gas is assumed to flow through the specimen in approximately hemispherical geometry and to the atmosphere. A tip seal made of soft rubber is used to prevent leakage between the probe and the specimen. Once steady state conditions are reached, the permeability measurement is computed using Darcy's equation and applying corrections for gas slippage and high velocity flow effects. The range of permeabilities measured can range from 0.1 milliDarcy to 3 Darcy[25].

Gas permeabilities were mapped for both arkose sandstone and brick specimens. The specimens tested, were similar, although not the same, to those used for the wicking experiment. The permeability values were obtained for both the flat sides of the cylindrical specimen. Figures 22 and 23 show the gas permeability data of the arkose specimen from the two flat sides. Plot (a) shows permeability as a function of spatial position. The darker areas represent positions of lower permeability. Data from plot (a) is reproduced in plot (b) such that permeability measurements corresponding to all Y-coordinates are plotted in logarithmic scale on the horizontal axis. All X-coordinates are plotted on the vertical axis. Plot (c) presents a distribution function of permeability, with the peak indicating the most likely value. The gas permeability values varied over about one order of magnitude.

Figure 23 presents data gathered on the other face of the arkose sandstone specimen in a format similar to that of Figure 22. Comparison of Figures 22 and 23 show differences in the gas permeabilities measured on the two ends of the cylindrical specimen. Figure 24 presents data gathered on one of the flat faces of the brick specimen, again in a similar format.

This method has a potential for providing very useful permeability data; however, some additional modifications would be required to be directly applicable for future work.

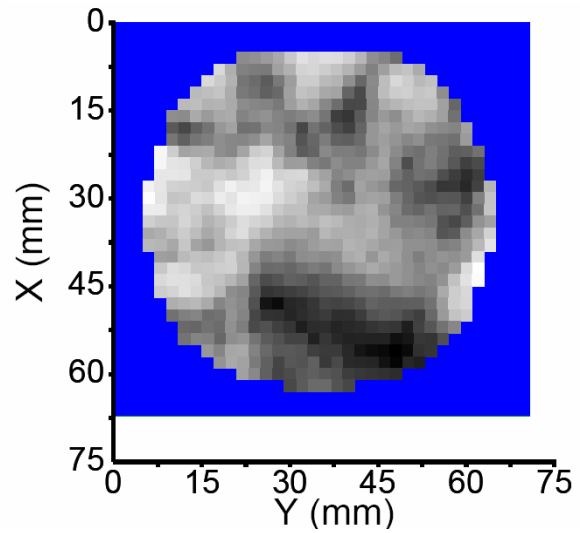

(a) Map of gas permeability

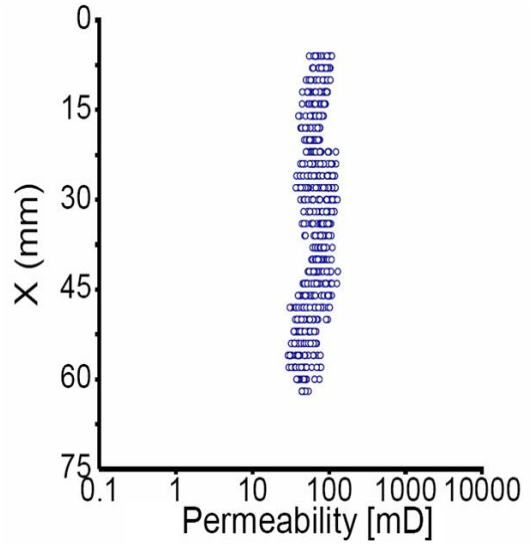

(b) Range of gas permeability

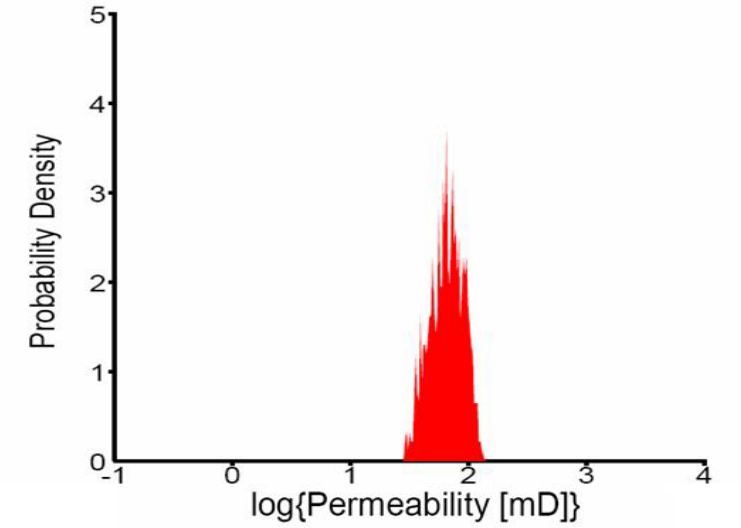

(c) Density function of gas permeability

Figure 22: Spatial variability of gas permeability of one face of the arkose sandstone specimen

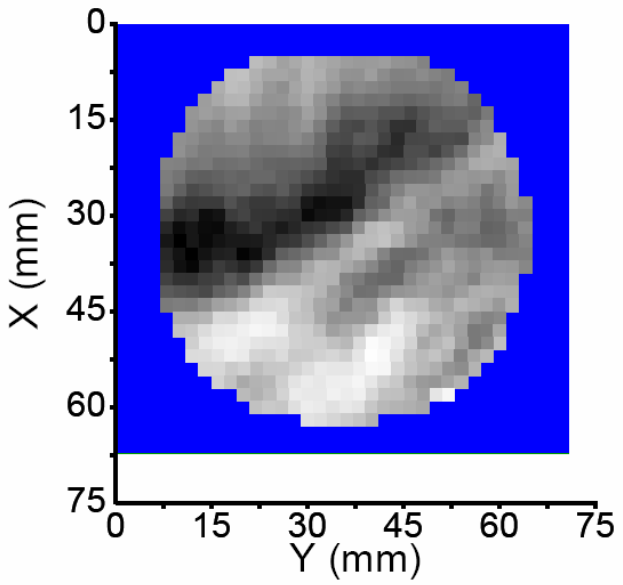

(a) Map of gas permeability

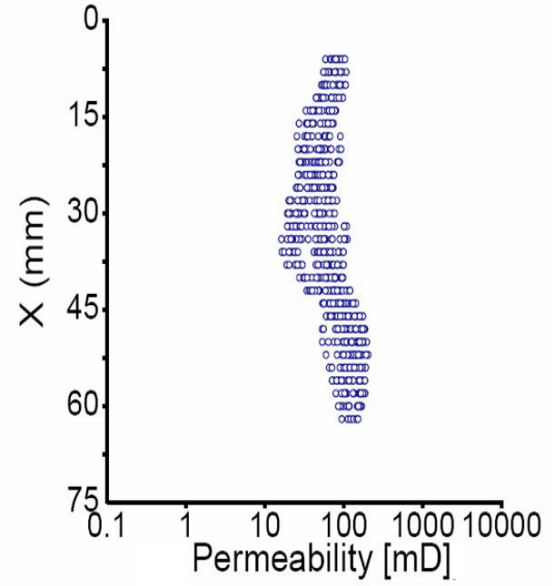

(b) Range of gas permeability

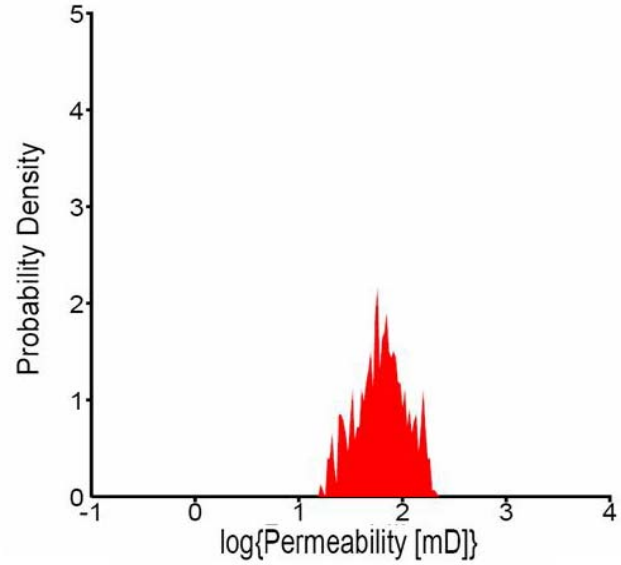

(c) Density function of gas permeability

Figure 23: Spatial variability of gas permeability of the opposite face of the arkose sandstone specimen

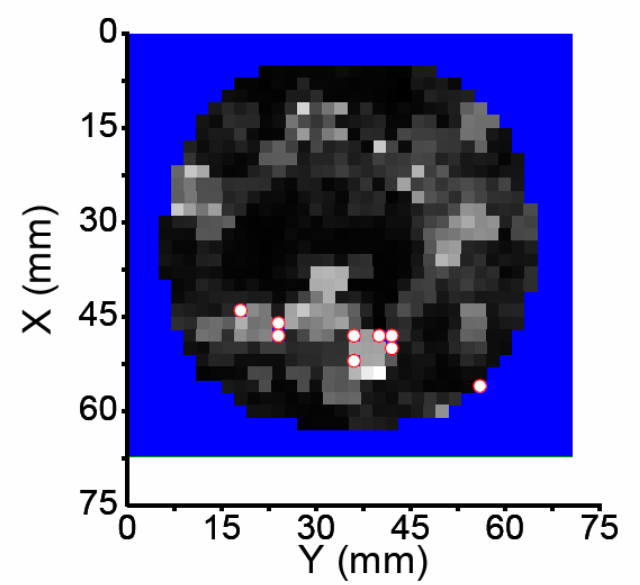

(a) Map of gas permeability

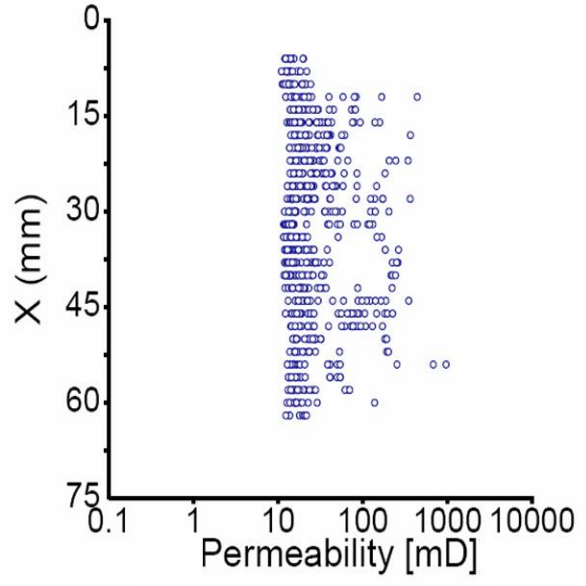

(b) Range of gas permeability

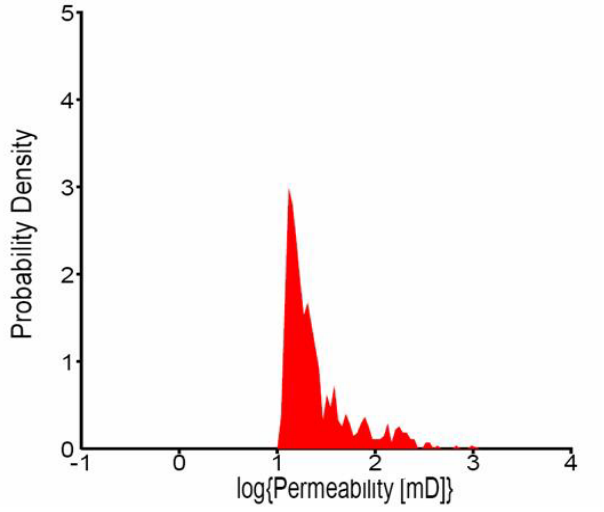

(c) Density function of gas permeability

Figure 24: Spatial variability of gas permeability of one of the flat faces of the brick specimen

SUMMARY AND CONCLUSIONS

This research provided information and the evaluation of six experimental techniques for application to investigating contaminating agents in building materials. The work was short-term and exploratory in nature but could be developed into a full-scale research project related to contaminating agents in building materials. The investigated experimental techniques can be divided into two groups based on the degree of complexity and needed equipment; relatively simple – contact angle, wicking, and dye migration experiment; and relatively complex – CT scanning, fluorescent confocal microscopy, and gas permeability mapping using an "autoscan".

The first group used simple experimental arrangements; and data were recorded using direct measurements, a digital camcorder or a microscope. The second group used state-of-the-art experimental techniques requiring special expertise and training.

Contact angle experiments: The contact angle experiments can provide information related to wetability. This is particularly important when investigating foam or gels that might be used in decontamination of building materials. Water was used in our experiments; however, other fluids may be used. The two materials for which drops formed on the dry materials, prior to being absorbed, were the two materials with the lowest imbibition rates. This is interesting because wetting behavior definitely affects capillarity. The contact angle method needs to be further explored to avoid instantaneous absorption of liquids. Considering that the experiments are fairly simple to conduct, measurements of contact angles should be attempted in the future.

Wicking experiments: The average imbibition rates for each specimen were calculated using experimental data from both bottom up and top down wicking experiments. The porosity of the specimens as reported in Ashworth, et al. (2005), as well as the average imbibition rates are summarized in Table 9. The amount of water absorbed by each specimen is also presented. The imbibition rates for a given material for the two test series were very similar as seen from Table 8 as well as the plots shown in Figures 4 through 9. It can be seen from Table 8 that each specimen absorbed a similar amount of water in both test series. The discrepancy seen with the arkose sandstone and Indiana limestone is a result of the different time periods that the experiments ran between test series I and II.

Figure 25 shows the correlation between the average imbibition rate and porosity of the specimens. As the porosity increases the rate of water imbibition also increases. The diamond marker corresponds to test series I and the circle marker is representative of test series II.

Wicking experiments provide one-dimensional examples of fluid transport in porous media. They are simple to conduct, yet provide a valuable set of measurements for verification of analytical methods. Therefore, they should be used in future studies.

Table 9: Imbibition rate, porosity, and amount of water absorbed for both test series

Material	Porosity	Average Imbibition Rate		Average Weight of Water Absorbed (g)	
		Test Series I	*Test Series II*	*Test Series I*	*Test Series II*
Arkose Sandstone	0.12	0.1333	0.0093	3.75	8.4
Indiana Limestone	0.125	0.3050	0.1577	10.15	15.05
Ohio Sandstone	0.18	0.6848	0.9739	22.7	23.25
Mortar	0.225	0.8458	1.0996	45.8	43.65
Brick	0.375	1.0786	1.1366	59.9	53.52
Concrete	--	2.1956	2.2852	62.25	59.7

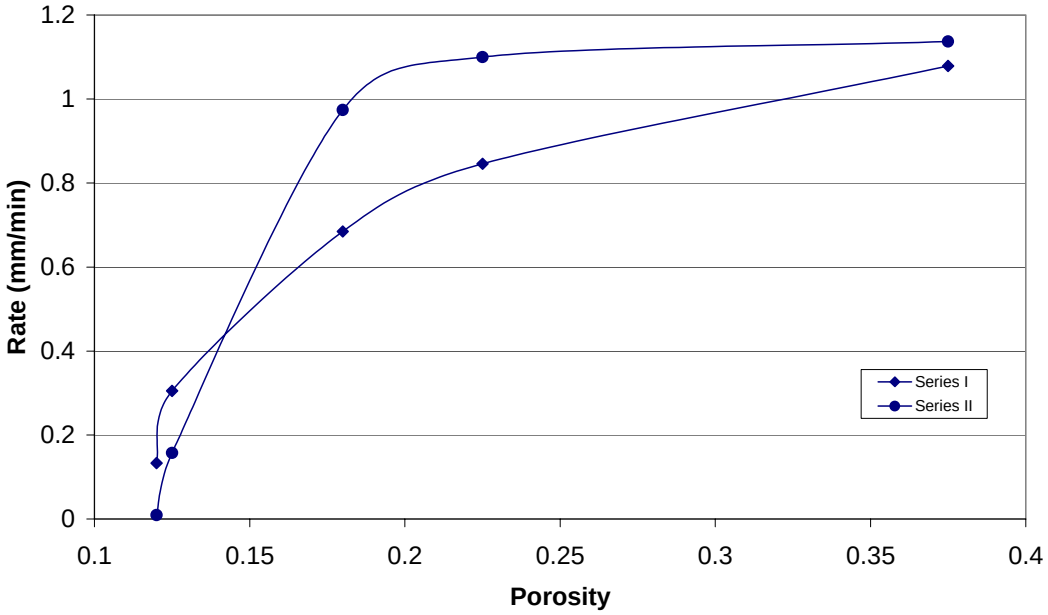

Figure 25: Average imbibition rate vs. porosity

Dye migration experiments: The dye migration experiment showed promise of generating good data for the two-dimensional physical model of fluid transport in a porous medium. If microscopic images are used, it may be possible to determine geomorphic pore structure using image analysis. It may also be possible to determine dye concentrations through image analysis. It is possible to simulate different geomorphic structures (e.g. pore distributions, cementation and initial moisture contents) using sand, clay and other materials, although these would still be only surrogate building materials. However, similar dye migration experiments should be conducted for future studies. Some exploratory work is needed to develop techniques for proper scanning.

CT scanning: The images produced from the X-ray scans provided an accurate visual representation of the pore structure of the core along very closely spaced sections (at a spacing of 1.51 μm). We were successful in determining the total porosity of individual slices using image processing filters. Pore structure and porosity of arkose sandstone changed significantly over a short distance of 0.1125 mm. We were able to detect iodine residues in the scans of concrete. It is quite possible to develop an automated scheme where the scanned images of individual slices are digitally processed to develop a three-dimensional view of the geomorphic pore structure to ultimately be able to quantify details of pore connectivity (effective porosity), heterogeneity and tortuosity. The technique should continue to be used for studying contaminant transport in building materials. Exploratory work is needed for optimizing settings for obtaining the best possible images.

Fluorescent confocal microscopy: Confocal microscopy proved to be an effective way of achieving visual representation of a material's pore structure (pore sizes and heterogeneity). The major limitation is that the laser can only reach approximately 0.2 mm depth into the specimen. In future studies, this method should be used as a complementary technique to the CT scanning; and image analysis could be done to determine porosity and pore structures for specific locations on the specimen.

Gas permeability mapping using "autoscan": In general, the gas permeability of materials (arkose sandstone and brick) determined using this method was one to two orders of magnitude higher than the saturated (with water) or gas permeability determined using constant head techniques (Ashworth, et al., 2005). It is to be noted that the autoscan determines the permeability on the surface using forced nitrogen, whereas, constant head tests were conducted under relatively small hydraulic gradients. The most useful feature of this technique is that it is capable of mapping the exposed surface of the porous material and detecting the degree of heterogeneity. It may be possible to convert this table top laboratory equipment into a portable piece of equipment for field use. The gas permeabilities can be correlated to the resistivity and seismic wave speeds, which the equipment is also capable of measuring. These quantities can be mapped before and after introducing contaminants and can also be correlated to depths to which the contaminants reach (which could be determined using CT scanning).

APPENDIX A

Agent Fate:
Chemical and biological contaminants and the transport properties of historic building materials

DRAFT REPORT
Phase 1: Experimental Research

Prepared by: Civil and Environmental Engineering and History
The University of Vermont
Burlington, VT

Project Team:
Lindsay Ashworth, Mandar Dewoolkar, Changfu Wei
Civil and Environmental Engineering

Douglas Porter, Thomas Visser, Rebecca Williams
History

Prepared for: Los Alamos National Laboratory
Materials Science Division
Los Alamos, NM

April 6, 2005

INTRODUCTION AND OBJECTIVES

The overall project objective is to develop and verify analytical models for predicting the long-term fate and transport of chemical or biological agents in building materials, in order to ultimately assist in the development of effective decontamination strategies. An understanding and characterization of physical interactions between agents and building materials, natural attenuation, evaporation/re-suspension rates, and the impact of the porosity on decontamination are required to achieve the above mentioned objective.

This report summarizes findings of Phase 1 experimental research conducted at the University of Vermont. The primary purpose of the experiments was to determine hydraulic properties of some representative building materials (stones, wood, brick and mortar). Determination of hydraulic conductivities of such materials was thought to be challenging because: (1) the range of conductivities can possibly be very broad, and may require changes in equipment and testing procedures; (2) the rigidity of the specimens may not be compatible with testing devices; and (3) of the connectivity and tortuosity of pores and the variability in pore structure in a given material. It was recognized that hydraulic conductivity may change drastically as a function of degree of saturation. However, before unsaturated hydraulic conductivity tests could be performed, an understanding of the behavior of these materials (with a wide range of hydraulic conductivities) was needed under saturated conditions, which provides an upper bound of hydraulic conductivity for a given material. In this phase of the research only the saturated hydraulic conductivity was considered with water as the permeating fluid. The future phases of research may consider hydraulic conductivity as a function of saturation and may use surrogate fluids to represent chemical and biological agents of interest.

The specific objectives of the research were to:

1. conduct a literature review;
2. select and prepare materials for testing;
3. perform absorption testing;
4. perform hydraulic conductivity testing with water as the pore fluid under saturated conditions;
5. perform pertinent index properties of selected building materials including specific gravity and porosity;
6. prepare a report describing the testing procedures, results, and analysis.

MATERIALS

Representative building materials found in high-value facilities and likely to interact with chemical agents were selected. Tests on a total of 18 specimens were conducted. A detailed description of these materials is given below.

Four types of porous building materials were tested: stone, brick, mortar, and wood.

The stone group was comprised of three different types of stone: (1) arkose sandstone, (2) Ohio sandstone, and (3) Indiana limestone. At least two samples of each material were tested. The stone samples originated from three different quarries and were each acquired from Granite Importers, Inc., located in Barre, Vermont. Each of the cylindrical stone samples was cut from the same original stone, and had a diameter of 2.75 inches and a height between 4 and 4.5 inches. The arkose sandstone came from the Portland Brownstone Company's quarries located in Portland, Connecticut. The stone is a deep purple-red stone with relatively large (2+ mm) multi-colored aggregate. The Ohio sandstone originated from the Waller Brothers Company in McDermott, Ohio. This sandstone is tan in color and is very fine-grained with small brown inclusions. The limestone was from the Oolitic, Indiana-based Indiana Limestone Company. The limestone is light gray, fine-grained, and has few inclusions.

A total of four brick samples were cored from two different late nineteenth-century bricks produced by the former Drury Brickyard in Essex, Vermont. Two cylindrical samples from each brick were used, each with a diameter of 2.75 inches and an average height of 2 inches.

The three mortar samples were made using a lime-based concrete mortar, based on an 8:1:1 ½ ratio of sand to Type 1 Portland cement to Type S dried hydrated lime. Enough tap water was added to produce a workable mixture. The mortar was poured into cylindrical molds to produce samples 2.75 inches in diameter and 5 inches in height. Placed in a concrete curing box at 72 ± 3°F, the samples were allowed to cure for one week.

The final type of material, wood, consisted of two cylindrical cores of beech wood, 2.75 inches in diameter and 4 inches in height, with the grain of the wood parallel to the axial direction of the cylinder.

EXPERIMENTAL PROCEDURES

The saturated hydraulic conductivity of the building stones, brick and mortar was measured in general accordance with ASTM D5084-00; Standard Test Methods for Measurement of Hydraulic Conductivity of Saturated Porous Materials Using a Flexible Wall Permeameter. The tests were accomplished using a Wykeham Farrance permeability cell and pressure panel (Figure 1).

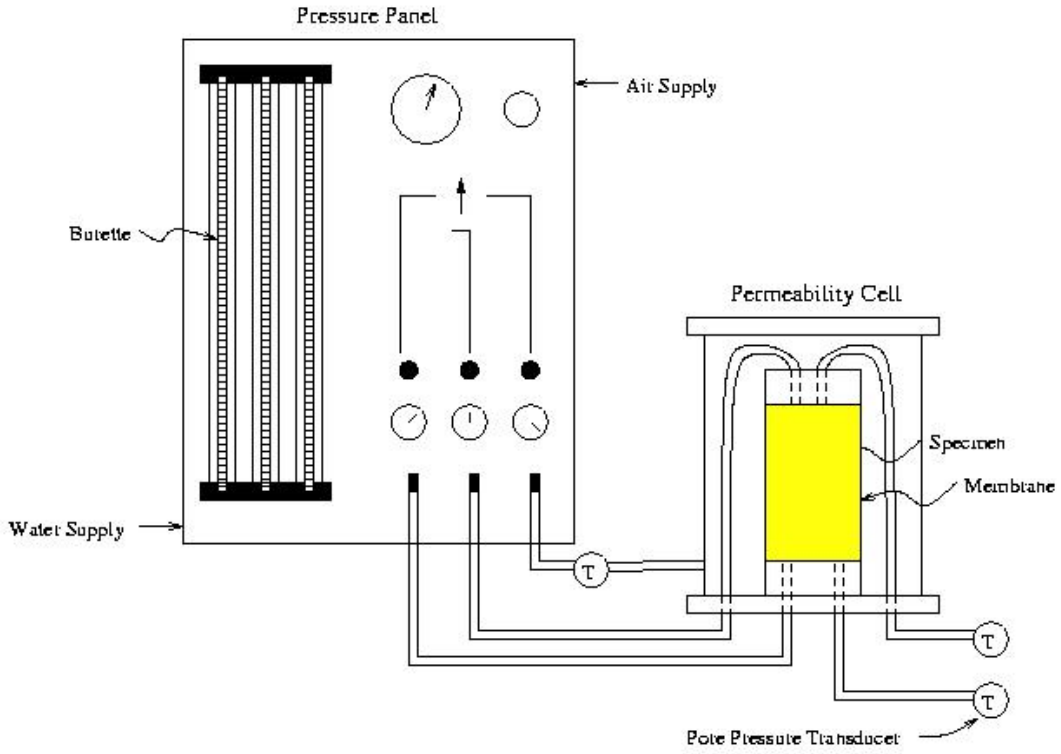

Figure 1: Apparatus used to perform water permeability tests

The samples were flushed with carbon dioxide before deaired water was flushed through the system, to aid in saturation. The degree of saturation was verified by measuring the B coefficient (as described in ASTM D 4767), a value of 0.95 was considered fully saturated. A constant pressure gradient was applied to the cylindrical sample to force flow from the bottom to the top of the sample. Two Geotest pressure transducers were used to measure the applied pressure gradient. A measured quantity of water was passed through the sample and the time elapsed was recorded and used to calculate the hydraulic conductivity using the following equation.

$$k = \frac{\Delta Q \cdot L}{A \cdot h \cdot \Delta t}$$

where:

k = hydraulic conductivity, m/s

ΔQ = quantity of flow for given time interval Δt, taken as the average of inflow and outflow, m^3

L = length of specimen, m

A = cross-sectional area of specimen, m^2

Δt = interval of time over which the flow ΔQ occurs, sec

The air permeability of the wood and mortar was measured in general accordance with ASTM D 4525-90; Standard Test Method for Permeability of Rocks by Flowing Air. It was decided to use air as the permeating fluid because of the swelling properties of wood, and the possible disintegration of the mortar in the presence of water. The Wykeham Farrance permeability cell was also used in these tests, with the two Geotest pressure transducers to measure the pressure drop across the sample (Figure 2). A regulated supply of compressed air was used to apply pressure to the bottom of the sample, while the exiting air flow was measured using a calibrated bubble flow meter.

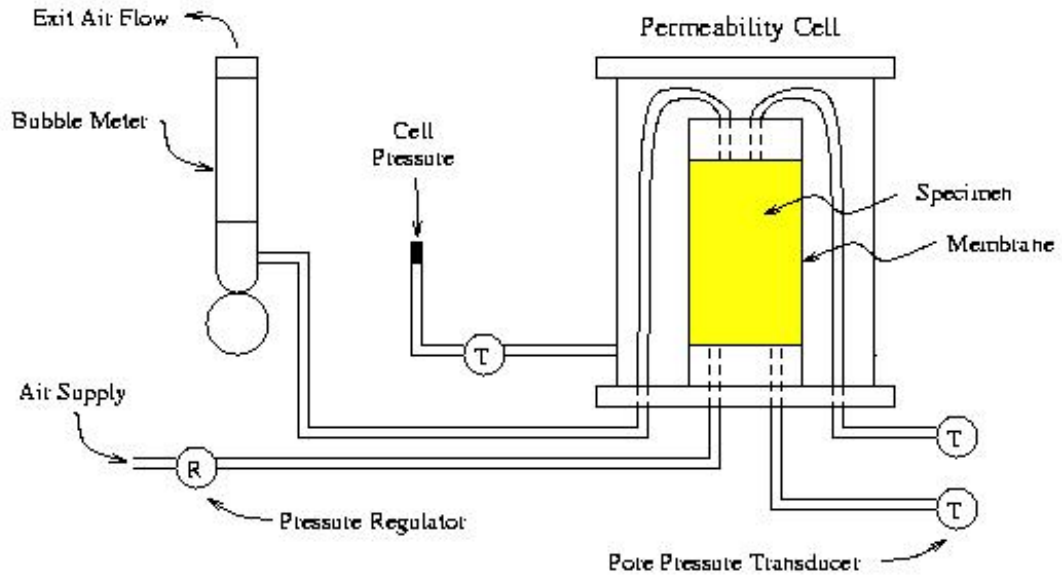

Figure 2: Apparatus used to perform air permeability tests

The absolute permeability was calculated using the following equation,

$$K = \frac{(2Q_e P_e \mu L)}{(P_i^2 - P_e^2)A}$$

where:

K = coefficient of permeability, m^2
Q_e = exit flow rate of air, m^3/s
P_e = exit pressure of air, Pa
P_i = entrance pressure of air, Pa
L = length of specimen, m
A = cross-sectional area of specimen, m^2
μ = viscosity of air at temperature of test, Pa·s

To obtain the equivalent liquid permeability of the wood and mortar specimens, the air permeability data was manipulated as recommended in the ASTM standard. The coefficient of permeability versus the reciprocal of the mean pressure was plotted and a linear regression line was used to connect the points, with the intercept representing the liquid permeability. The intercept represents the point of infinite pressure, where all gases would become a liquid. The air permeability of one sample of each stone was also measured to validate correlation between the hydraulic conductivity calculated from the air permeability measurements and the hydraulic conductivity measured directly with the permeameter. In each case, the hydraulic conductivity of the stone specimen with water was very close to the one computed based on air permeability measurements.

The absorption and specific gravity of all the non-organic samples (stone, mortar and brick) was measured in general accordance with ASTM C 97- 02; Standard Test Method for Absorption and Bulk Specific Gravity of Dimension Stone. The samples used in the permeability tests were cut to the recommended size before performing the absorption and specific gravity measurements. The absorption test involved completely drying the samples in a drying oven and then immersing them in distilled water for 48 hours. Although the standard did not require it, the samples were saturated under a vacuum for 24 hours in order to maximize saturation of the void spaces. The samples were weighed dry and again after immersion. The absorption was calculated as the ratio of the weight of water absorbed to the weight of the dry sample.

The bulk specific gravity of the sample was then found by suspending the saturated sample in water and measuring the suspended weight. The specific gravity was calculated using the following relationship,

Bulk specific gravity = A/(B - C)

where:
A = mass of the dry sample, g
B = mass of the sample after immersion, g
C = mass of the soaked specimen in water, g

The specific gravity of the wood samples was measured in general accordance with ASTM D 2395-02; Standard Test Methods for Specific Gravity of Wood and Wood-Based Materials. Using method A of the standard test method the specific gravity was found by measuring the volume, mass and moisture content of the sample and using the following equation,

$$Bulk\ specific\ gravity = W/[1 + (M/100)]V$$

where:
W = weight of the specimen, g
M = moisture content of the sample, %
V = volume of the sample, cm^3

The porosity of the non-organic materials was calculated using previously collected information and the measured volume of the samples. The porosity is defined as the ratio of the volume of voids to the total volume of the sample.

RESULTS

Hydraulic conductivity values were determined through both water and air permeability tests. The results of all tests are summarized in Table 1. For wood, mortar, and sample #4 of the arkose sandstone the values reported in Table 1 are the hydraulic conductivity deduced from air permeability data. A range of typical values found in published literature are also given in the following tables. Due to the natural variability of the materials tested, the published values cover a large range. In most cases the values found were within the range or at least within the order of magnitude of the published values.

Table 1: Hydraulic conductivity values of each sample and a comparison to published data.

Material	**Hydraulic Conductivity** (m/s)				**Published** *(m/s)*	**Reference**
	Sample 1	*Sample* 2	*Sample* 3	*Sample* 4		
Arkose sandstone	1.6E-09	5.8E-10	1.1E-08	3.4E-09	1E-07 to 1E-01	[1]
Ohio sandstone	4.9E-07	6.0E-07	5.3E-07	-	1E-07 to 1E-01	[1]
Indiana limestone	7.4E-09	1.2E-08	-	-	2.5E-09 to 2.5E-06	[2]
Brick	7.7E-08	8.1E-08	3.7E-08	3.7E-08	3.8E-09 to 3.2E-08	[2]
Mortar	4.9E-08	8.6E-08	7.3E-08	-	4.6E-11 to 3.7E-10	[3]*[2]**
Wood	6.7E-05	7.9E-05	-	-	3E-07 to 5E-05	[4]

* 1 part Portland cement, ½ part hydrated lime, 3.5 – 4.5 parts aggregate
** 1 part cement, 3 parts sand

Table 2: Correlation between water and air permeability tests.

Sample	**Permeant**	**Hydraulic Conductivity** *(m/s)*
Arkose Sandstone(ave)	Water	4.5E-09
Arkose Sandstone -4	Air*	3.4E-09
Ohio Sandstone -1	Water	4.9E-07
Ohio Sandstone -1	Air*	8.7E-07
Indiana Limestone -1	Water	7.4E-09
Indiana Limestone -1	Air*	1.6E-08

* deduced from using air permeability

In order to verify the assumption that the air permeability test would provide for adequate hydraulic conductivity measurements, one sample of each type of stone was dried completely and retested in the air permeability apparatus. The coefficient of permeability was determined and then converted to a hydraulic conductivity; this result was compared with the hydraulic conductivity obtained with the water permeability apparatus. An example of the extrapolation from the coefficient of permeability to hydraulic conductivity can be seen for the mortar (sample 2) in Figure 3. Table 2 shows very close correlation between the results from either test.

The specific gravity of the beech sample was found to be 0.72 using the average of two samples. The absorption, specific gravity, and porosity results of all the inorganic materials are summarized in Table 3 as well as a comparison to published values.

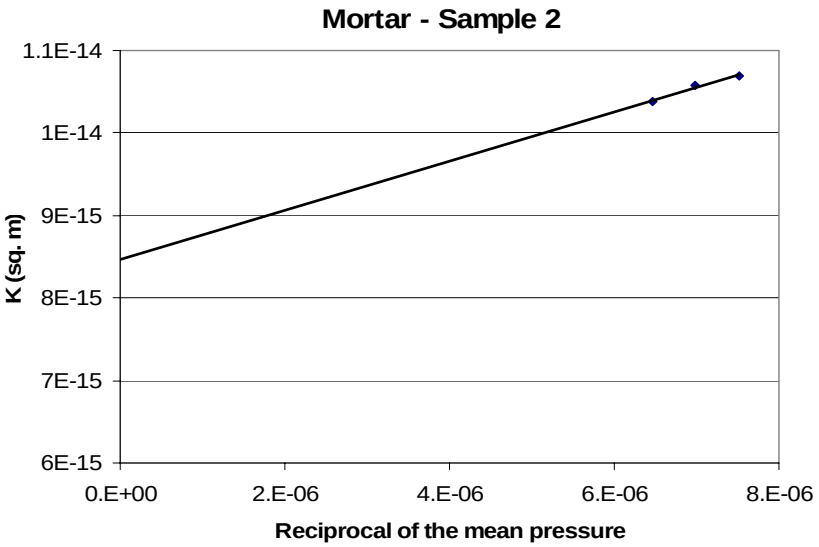

Figure 3: Extrapolation from coefficient of permeability to hydraulic conductivity

Table 3: Average Absorption and Specific Gravity Results

Sample	**Absorption** *(%)*	**Bulk Specific Gravity**	**Published Bulk Specific Gravity**	**Porosity**	**Published porosity**
Arkose sandstone	4.9	2.39	1.95-2.15	0.12	.085-.24
Ohio Sandstone	8.4	2.17	1.95-2.15	0.18	.085-.24
Indiana Limestone	5.3	2.36	2.01-2.24	0.125	.176-.245
Mortar	12.2	1.84	2.07	0.225	0.167-0.310*
Brick	22.4	1.66	1.69	0.375	.070-.359

1. Absorption, bulk specific gravity and porosity results are average of two samples, except brick which is an average of four samples.
2. [2] except * which is [3]

CONCLUSIONS

Four types of representative building materials were tested; stone, brick, mortar and wood. The properties determined for each of the materials were the hydraulic conductivity, absorption, specific gravity and porosity. The hydraulic conductivity of stone and brick was found using a flexible walled permeameter with water as the pore fluid. The hydraulic conductivity of mortar and wood was found using the same flexible walled permeameter with air as the pore fluid. Good correlation was demonstrated between these two tests, and the results were compared with published literature. Absorption was found for the stone, brick and mortar samples. The specific gravity was found for the stone, brick, mortar and wood; and was compared to published values. The results were generally within the ranges of values in published literature for similar materials.

In order to complete the objectives of this research, the hydraulic conductivity and capillary pressure of the materials as a function of saturation should be found. This will be possible with modification of the equipment used in this phase. This is recommended as phase 2 of the research.

REFERENCES

1. Bourbie, T. and B. Zinszner, *Hydraulic and Acoustic Properties as a Function of Porosity in Fontainebleau Sandstone.* Journal of Geophysical Research, 1985. **90**(B13): p. 11,524-11,532.
2. Hall, C. and W.D. Hoff, *Water Transport in Brick, Stone and Concrete*. 2002: Spon Press.
3. Kumaran, M.K., et al., *Heat, Air and Moisture Transport Properties of Several North American Bricks and Mortar Mixes.* Journal of Testing and Evaluation, 2004. **32**(5): p. 383-389.
4. Comstock, G.L., *Longitudinal Permeability of Wood to Gases and Nonswelling Liquids.* Forest Products Journal, 1967. **17**(10): p. 41-46.